

Chapter 5

Heat-Integrated Intensified Distillation Processes

J. Rafael Alcántara-Avila and Hao-Yeh Lee

Abstract Heat integration between vapor and liquid streams has been widely used in chemical and petrochemical plants for conventional distillation processes as an alternative to reduce the energy consumption. However, with the advances that have been proposed in intensified distillation processes in the last couple of decades, heat-integrated alternatives that are more attractive than the typical condenser–reboiler heat integration have also been proposed. Therefore, intensified distillation processes also need a new approach methodology to implement optimal locations and heat load in heat-integrated distillation. This chapter aims to cover the fundamentals, simulation and optimization approaches for heat-integrated intensified distillation processes for nonreactive and reactive systems. Conventional distillation can result in an intensified process if heat integration is allowed at locations other than the condenser and reboiler. Although thermally coupled distillation and Heat-Integrated Distillation (HIDiC) are already intensified processes, they can attain higher energy reduction by rearranging their heat load distribution. For reactive systems, at the location subject to heat integration, vapor–liquid equilibrium and reaction kinetic conditions are modified simultaneously, which results in a very challenging problem. Reactive system via multi-effect and thermally coupled configuration is also covered in this chapter for the methyl acetate hydrolysis and esterification of isopropyl alcohol. The applications of heat-integrated intensified distillation show feasible solutions with improved energy efficiency and total annual cost reduction for new designs.

J.R. Alcántara-Avila (✉)
Tokushima University, 2-1 Minami Josanjima-cho, Tokushima 770-8506, Japan
e-mail: jrafael.alcantara@tokushima-u.ac.jp

H.-Y. Lee
National Taiwan University of Science and Technology, Taipei City, Taiwan

5.1 Fundamentals in Heat Integration

Distillation is a process that repetitively boils liquid streams and condensates vapor streams from bottom to top at each stage for the separation of components with different vapor pressures. Components with lower vapor pressure are concentrated at the top of the column while components with higher vapor pressure are concentrated at the bottom of the column. Pressure and temperature gradients at each stage inside the column result in changes in the vapor–liquid proportion among components, therefore, separation is possible. The vapor leaving at the top of the distillation column is at the lowest temperature, and it is condensed by exchanging heat with a cooling utility (e.g., water) in a device called condenser. Contrarily, the liquid leaving at the bottom of the distillation column is at the highest temperature, and it is boiled by exchanging heat with a heating utility (e.g., steam) in a device called reboiler.

To reduce the necessary amount of cooling and heating utilities in distillation, one possibility is to use the column streams to provide cooling or heating; therefore, vapor streams above the feed stage (i.e., rectifying section) can be regarded as vapor heat sources and liquid streams below the feed stage (i.e., stripping section) can be regarded as liquid heat sinks [1]. However, the necessary condition to realize heat integration in distillation columns is that the temperature of heat sources must always be higher than that of heat sinks by at least a specified minimum temperature difference ΔT_{\min} . To satisfy this condition, the pressure and/or the temperature of only the top vapor stream or the entire rectifying section must be increased.

5.1.1 Heat-Integrated Distillation

Although condenser–reboiler heat exchange has been widely used in the last couple of decades, the pressure difference between the condenser and reboiler must be at its maximum value to satisfy a given ΔT_{\min} .

The heat-integrated distillation processes presented in this chapter exploit the idea of removing heat from stages in the rectifying section, which are at a temperature higher than that in the condenser, and supplying heat to stages in the stripping section, which are at a temperature lower than that in the reboiler. Thus, the search space for optimal distillation processes is expanded by including the heat integration possibilities between stages in rectifying and stripping sections in the same column or in different columns.

Figure 5.1 shows a representative temperature profile for the separation of 100 kmol/h a benzene-toluene equimolar mixture into two products with 99 % mol purity. The vertical axes show the temperature profile for heat sources in the rectifying section at the left and that for heat sinks in the stripping section at the right, respectively, and the horizontal axis shows the stage number. In addition, stages are numbered from the top condenser (stage 1) to bottom reboiler (stage 20).

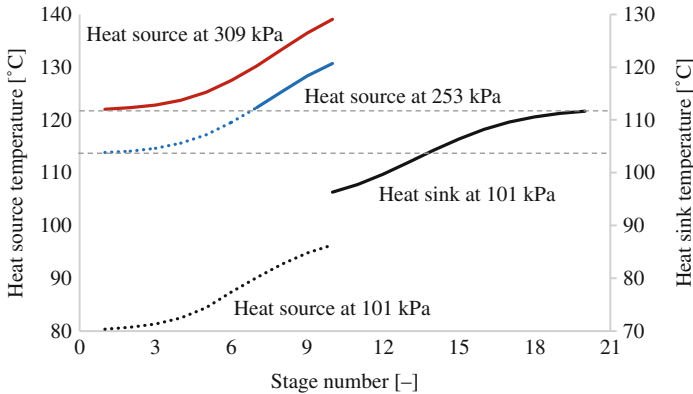


Fig. 5.1 Rectifying and stripping section temperature profile for a benzene/toluene separation

The solid lines in Fig. 5.1 represent feasible heat integrations while the dotted lines represent infeasible heat integrations with the reboiler. Additionally, the assumed value of ΔT_{\min} is 10 °C. To realize heat integration between the vapor stream at stage 1 and the liquid stream at stage 20, the pressure must be equal or higher than 309 kPa. If heat sources are at a lower pressure (253 kPa), the condenser–reboiler heat integration becomes infeasible, but it is still possible to exchange heat between vapor streams in the condenser and liquid streams from stage 10 to stage 13, and vapor streams from stage 7 to stage 9 and the liquid stream in the reboiler.

5.1.2 Problems in Simulation and Optimization of Heat-Integrated Distillation

There are three main differences between conventional condenser–reboiler heat integration (i.e., external heat integration) and heat integration between stages (i.e., internal heat integration) [2]. Because of these differences, simulation and optimization problems have been limited for the heat integration between two sections in the same column or between two different columns for the separation binary and multicomponent mixtures [1–4].

5.1.2.1 Combinatorial Problem

There is a remarkable increase of heat integration possibilities when stages are considered as candidates for heat integration, and it is represented in Fig. 5.2. The typical case of heat integration is the one between condenser and reboiler (Fig. 5.2a). In the case of heat integration between stages, heat can be supplied from all the M stages in a rectifying section to all the N stages in a stripping section.

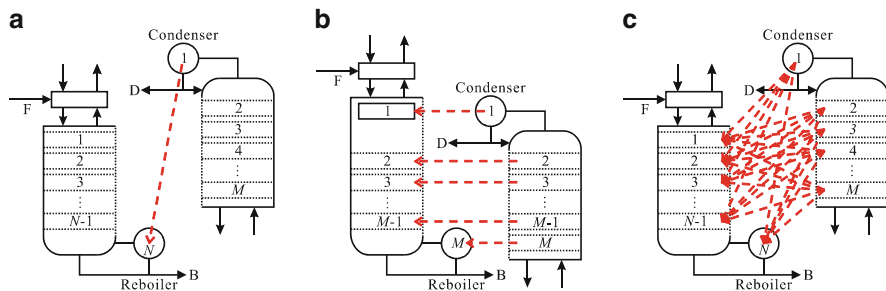


Fig. 5.2 Heat integration possibilities between rectifying and stripping sections. (a) Condenser-reboiler. (b) Internal heat integration one to one. (c) Internal heat integration one to all

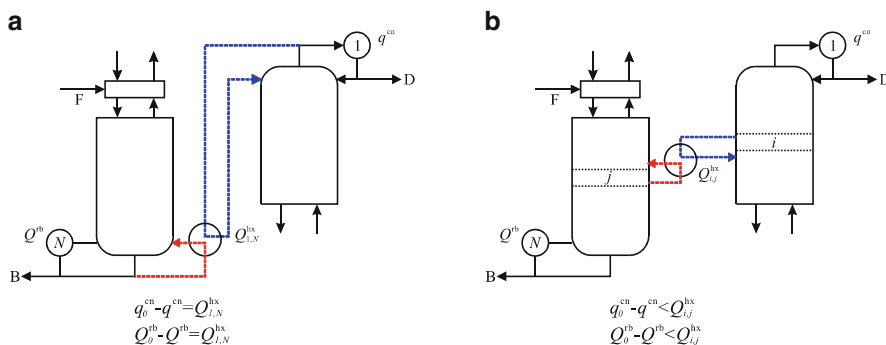


Fig. 5.3 Changes in heat duty after heat integration. (a) Between condenser and reboiler. (b) Between stages

In Fig. 5.2b, heat integrations can be done from one stage in the rectifying section to one stage in the stripping section while in Fig. 5.2c heat integrations can be done from one stage in the rectifying to all stages in the stripping section, and vice versa. It can be seen that all combinations in Fig. 5.2a, b are included in Fig. 5.2c. Additionally in Fig. 5.2, F denotes the feed, D the distillate product, and B the bottoms product.

To illustrate how the combinatorial problem increases, consider that the rectifying section consists of ten stages ($M = 10$) and the stripping section consists of ten stages ($N = 10$), the possible matches in Fig. 5.2a–c are 1, 10, and 100, respectively, when one heat integration is enforced. If more heat integrations are enforced, the number of possible combinations also increases.

5.1.2.2 Changes in Heat Duty

There are changes in the condenser and reboiler heat duties after heat integration, and it is represented in Fig. 5.3. In the case of heat integration between a condenser and reboiler, their energy reduction is equal to the energy exchanged

between them (Fig. 5.3a). Contrarily, in the case of internal integration at stages, the energy reduction at a condenser and at a reboiler is not equal to the energy exchanged by the stage-stage heat integration (Fig. 5.3b).

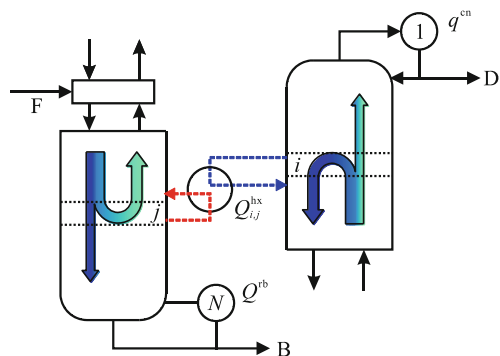
In Fig. 5.3, q_0^{cn} and Q_0^{rb} are the condenser and reboiler heat duty before any heat integration, q^{cn} and Q^{rb} are the condenser and reboiler heat duty after heat integration, and $Q_{i,j}^{\text{hx}}$ is the amount of heat exchanged between stages i and j . When heat is exchanged between the condenser ($i = 1$) and reboiler ($j = N$), the amount of heat reduced at the condenser and reboiler is equal to the amount of heat transferred $Q_{1,N}^{\text{hx}}$. Contrarily, when heat is exchanged between stages i and j , the amount of heat reduced at the condenser and reboiler is less than the amount of heat transferred $Q_{i,j}^{\text{hx}}$. Furthermore, the reduction in condenser and reboiler heat duties depends on two factors: the locations i and j subject to heat integration and the amount of heat transferred $Q_{i,j}^{\text{hx}}$.

5.1.2.3 Changes in Temperature Profile

The installation of heat exchangers in rectifying and stripping sections results in changes of the stage temperature due to the partial condensation and evaporation of components with higher and lower boiling points, respectively.

Figure 5.4 shows a conceptual representation of the partial evaporation and condensation of components in stages with heat integration. The degradation of arrows from dark to light represents the composition changes of components from higher to lower boiling point. In the rectifying section, while the components with a higher boiling point are partially condensed, the components with low boiling point move towards the top of the column. As a consequence, the stage temperature decreases because the composition of lower boiling point components increases. Contrarily in the stripping section, while the components with a lower boiling point are partially evaporated, the components with high boiling point move towards the bottom of the column. As a consequence, the stage temperature increases because the composition of higher boiling point components increases.

Fig. 5.4 Partial evaporation and condensation in heat-integrated stages



These temperature changes are difficult to estimate and to calculate because changes in the composition and temperature depend on the locations i and j subject to heat integration and the amount of heat transferred Q_{ij}^{hx} .

Because of the aforementioned differences between typical condenser–reboiler heat integration and heat integration at stages, the design, simulation, and optimization of intensified distillation processes through heat integration become more difficult. In the following sections, simulation and optimization approaches are proposed and validated through case studies in which the heat-integrated alternatives are better from the energy and economic viewpoints.

5.2 Simulation and Optimization of Heat-Integrated Intensified Distillation

Simulations can readily be done by process simulators or numerical analysis software. In process simulators, the governing equations for chemical processes and equipment are embedded in an object-oriented or equation-oriented environment while in the numerical analysis software, the process and equipment model must be programmed by the user. Similarly, optimization can be done by using built-in tools in process simulators, built-in tools in optimization software, or by programming an optimization algorithm.

Recent developments in process simulation and optimization techniques have facilitated its combined application to solve complex problems. However, in most cases, the use of built-in optimization tools in process simulators are limited to the solution of nonlinear constrained or unconstrained problems involving only continuous variables. In addition, convergence is difficult and usually fails to find feasible solutions.

This section presents a simulation-based optimization to find optimal heat-integrated intensified distillation processes by combining a mixed integer linear programming (MIP) optimization algorithm that can deal with all combinatorial problems (Sect. 5.1.2.1) and a process simulator that can deal with all the inherent nonlinearities and nonconvexities in distillation (Sects. 5.1.2.2 and 5.1.2.3) to find the optimal heat-integrated distillation process for nonreactive and reactive systems. The presented approaches in the next sections can effectively substitute trial-and-error approaches based on extensive simulations and complex mixed integer nonlinear programming problems (MINLP).

5.2.1 *Simulation and Optimization for Nonreactive Systems*

It is necessary to determine the objective function. When well-known equipment is used, or there is reliable data to estimate the cost, economic minimization should be preferred. However, when nonstandard equipment is used, or there is a high

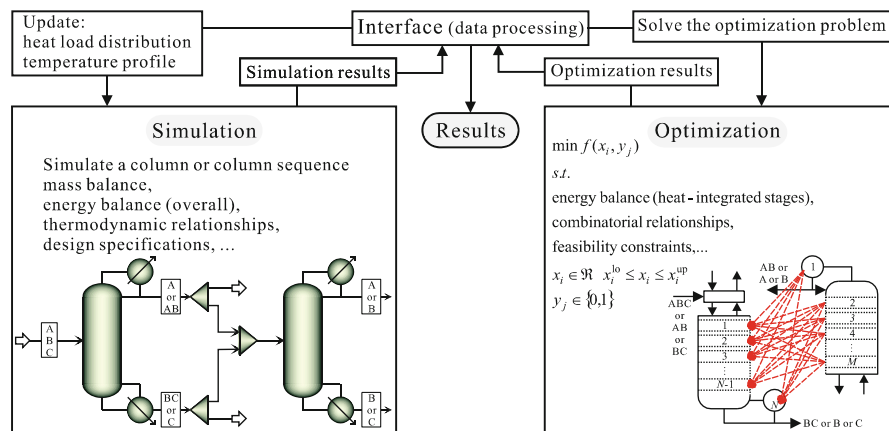


Fig. 5.5 Simulation-based optimization approach for nonreactive systems

uncertainty in their cost, energy minimization should be preferred. Although the minimization of economic and energy criteria is dominant, entropy production, environmental impact, or another criterion can be chosen without any major changes in the optimization procedure.

In Sect. 5.3.1 the objective function is to minimize the cost and energy requirement, the continuous variables are the vapor flow rate and its pressure and temperature at the compressor outlet and at each heat-integrated stage, and the integer variables are the locations and the number of compressors and heat-integrated stages. In Sects. 5.3.2, 5.3.3, and 5.4.2, the objective function is to minimize the energy, the continuous variables are the pressure at each section, the vapor flow rate to the compressor, and the heat distribution in heat-integrated distillation column (HIDiC), and the integer variables are the locations and the number of heat-integrated stages (Sects. 5.3.3 and 5.4.2).

The optimization approaches to design HIDiC in Sect 5.3 use extensive simulations or graphical methods for the separation of binary or multicomponent mixtures into two product streams. The proposed optimization approach in this chapter to find heat-integrated intensified distillation is described in Fig. 5.5. It takes the advantages from mixed integer linear optimization to find the locations of heat-integrated stages and the robustness of process simulation to deal with all the inherent nonlinearities and nonconvexities in distillation.

In Fig. 5.5 a column simulation can be a HIDiC or one with vapor recompression while a column sequence simulation can be a conventional sequence or a thermally coupled configuration for the separation of multicomponent mixtures. The simulation and optimization variables are solved iteratively until they converge to the final results. The involved variables in the simulation are continuous (e.g., pressure, temperature, molar flow, liquid or vapor composition) and integer (number of stages, feed stage) while in the optimization x_i are the continuous variables (e.g., heat load distribution) and y_j are the integer variables (e.g., number of heat

exchangers, location(s) of heat-integrated stages). x_i^{lo} and x_i^{up} are the lower and upper bounds for continuous variables. Microsoft Excel can be used as an interface to handle the data between the simulation and optimization.

5.2.2 Simulation and Optimization for Reactive Systems

For reactive systems, the simulation and optimization approach is similar to the one in Fig. 5.5; however, there are some important features that must be considered in reactive systems. Unlike for nonreactive systems, the conversion is the most important factor when the stream leaves the reactive distillation. Otherwise, the whole system will not meet the composition specifications and even some of the continuous variables (e.g., reflux ratio, reboiler duty) will be used to adjust the product compositions. Therefore, the number of reactive stages and the holdup in the reactive stage need to be considered carefully before the optimization procedure.

A large reactive holdup is required to initialize the reactive system simulation. After this, the column diameter can be calculated in the process simulator. By using this diameter and the setting of the weir height, the holdup of each stage can be determined. As for the reactive section of the column, the catalyst volume in each tray is assumed to occupy half of the total holdup.

The proposed optimization approach in this chapter to find heat-integrated intensified reactive distillation is described in Fig. 5.6. It assumes complete conversion of reactants to products. It can also be seen that reactive holdup and number of trays can be updated and solved iteratively until it converges.

The simulation of reactive systems is not easy to converge to feasible results because of the complexity of reaction kinetics and thermodynamics. Due to the

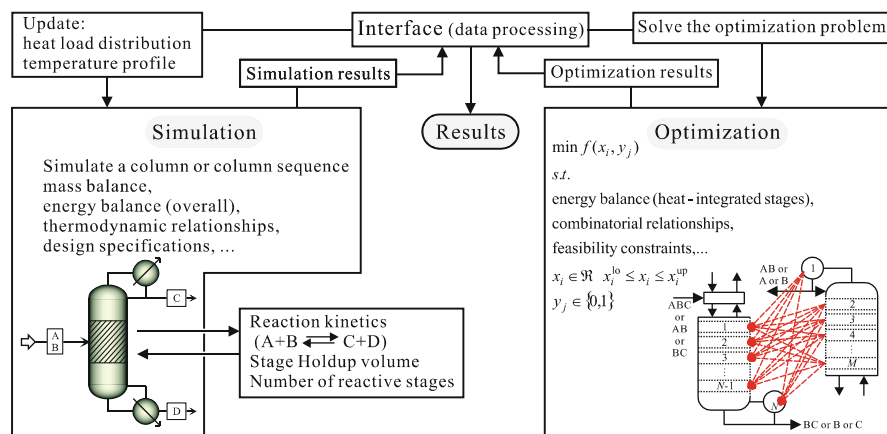


Fig. 5.6 Simulation-based optimization approach for reactive systems

complexity of reactive system characteristics, the optimization of these kinds of reactive distillation with heat integration is usually determined by sequential iterative methods. It means that the design variables need to be analyzed first and then run the simulations one at a time to find the optimal result.

5.3 Heat Pump-Assisted Distillation

Heat pump-assisted distillation processes have been proposed to reduce the energy consumption in distillation by increasing the pressure and temperature of the vapor streams in the rectifying section to exchange heat with the liquid streams in the stripping section. The vapor recompression is used to upgrade the heat by compressing the vapor distillate or a working fluid while the internally HIDiC enhances both heat and mass transfer [5]. In this section, the aforementioned applications and their working principles are covered.

5.3.1 Vapor Recompression Columns (VRC)

Conventional mechanical vapor recompression and vapor compression columns (MVR and VC) require either work input or external driving thermal energy to remove the heat from a low-temperature source and to transform it to a higher temperature level [6]. Figure 5.7 shows the working principle for MVR and VC in which a liquid boils or a vapor condenses at a higher temperature if its pressure is increased. In the figure, the low-pressure vapor passes through the compressor where it is compressed to a higher pressure by the application of work.

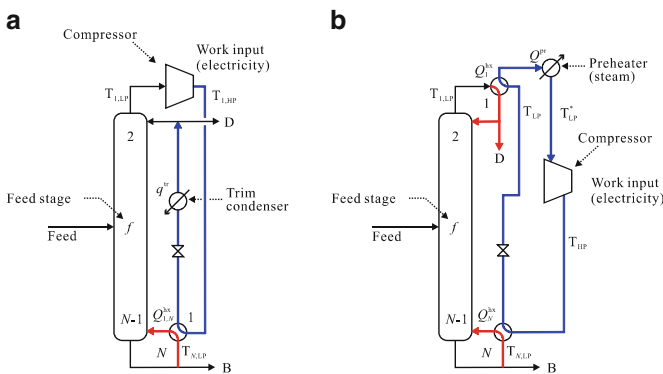


Fig. 5.7 Vapor recompression columns. (a) MVR. (b) VC

The resulting high-temperature vapor gives its latent heat at a high temperature to the low-pressure liquid causing it to boil. Then, the condensed liquid passed through a throttle valve and expands back to a low-pressure liquid. Figure 5.7a uses its own vapor streams while Fig. 5.7b uses an external fluid in the vapor compression cycle.

In Fig. 5.7a, the vapor leaving the column at low temperature ($T_{1,LP}$) is recompressed to reach an outlet temperature ($T_{1,HP}$) that must be higher than the liquid inlet temperature ($T_{N,LP}$) in the bottom stage to generate the heat integration $Q_{1,N}^{hx}$. After decompression of the reflux liquid stream a trim condenser (q^r) is used to returned the stream as a saturated or subcooled liquid.

In Fig. 5.7b, the vapor and liquid streams leaving the column at low temperature ($T_{1,LP}$ and $T_{N,LP}$) are condensed and boiled, respectively, by means of an external vapor compression cycle. In this case, the vapor temperature after compression (T_{HP}) must be higher than the liquid inlet temperature ($T_{N,LP}$) and the liquid temperature after the throttling valve (T_{LP}) must be lower than the vapor inlet temperature ($T_{1,LP}$) to generate the heat integrations Q_1^{hx} and Q_N^{hx} , respectively. After Q_1^{hx} , a preheater (Q^{pt}) is used to return the working fluid to the compressor as a saturated or superheated vapor at a temperature T_{LP}^* .

Economic and/or energy savings have been reported for MVR to recover chemicals in wastewater streams [7] and the separation of binary mixtures [3, 8], and for VC to the separation of binary mixtures [9]. In MVR and VC, the vapor stream is compressed until it reaches a temperature higher than that in the reboiler and cooled down at a temperature lower than that in the condenser; therefore, the compressor temperature and pressure differences are at their highest values ($T_{1,HP} - T_{1,LP}$ for MVR, and $T_{HP} - T_{LP}^*$ for VC), which can result in high compression work duty, thus high electricity cost. In the following subsections, heat-pump distillation processes with two-staged recompression and heat-integrated stages are covered in detail.

5.3.1.1 MVR with Heat-Integrated Stages

By reducing the temperature and pressure difference in the inlet and outlet streams in the compressor, savings in work duty and electricity can be attained. Figure 5.8a shows the heat integration possibilities between the top vapor stream leaving the column and stages in the rectifying section. For MVR with heat-integrated stages, it is necessary to use a trim reboiler (Q^r) to provide the remaining heat duty to achieve the desired product purity. Equation (5.1) shows the temperature relations between MVR and MVR with heat-integrated stages in the left and right side, respectively.

$$T_{N,HP} - T_{1,LP} > T_{j,HP} - T_{1,LP} \quad j \in f + 1, \dots, N - 1 \quad (5.1)$$

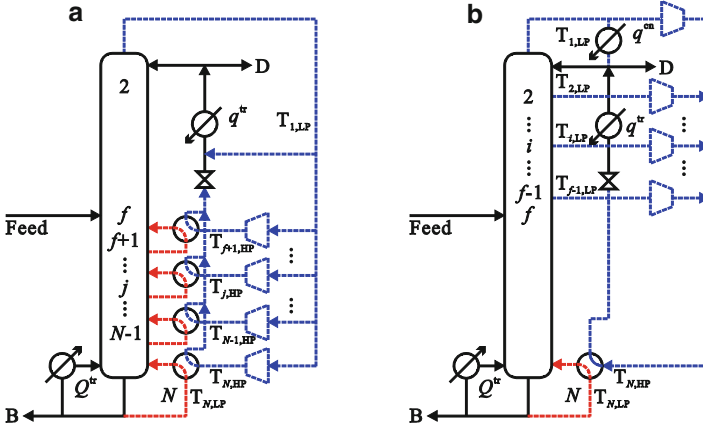


Fig. 5.8 Vapor recompression with heat-integrated stages. (a) Stripping section. (b) Rectifying section

Assuming an ideal, isentropic, diabatic expansion the compressor outlet temperature can be calculated as shown in Eqs. (5.2) and (5.3) for MVR and MVR with heat-integrated stages in the stripping section

$$T_{N,HP} = T_{1,LP}(P_{N,HP}/P_{1,LP})^{(\gamma-1)/\gamma} \quad (5.2)$$

$$T_{j,HP} = T_{1,LP}(P_{j,HP}/P_{1,LP})^{(\gamma-1)/\gamma} \quad j = f + 1, \dots, N - 1 \quad (5.3)$$

where $P_{N,HP}$, $P_{j,HP}$, and $P_{1,LP}$ are the high pressure at stage N , j and the low pressure at stage 1, respectively. $\gamma = Cp/Cv$ is called isentropic exponent. By combining Eqs. (5.1)–(5.3), it can be demonstrated that $P_{N,HP} > P_{j,HP}$.

Figure 5.8b shows the heat integration between vapor streams at stages in the rectifying section and the bottom liquid stream. Equation (5.4) shows the temperature relations between MVR and MVR with heat-integrated stages in the left and right side, respectively.

$$T_{N,HP} - T_{1,LP} > T_{N,HP} - T_{i,LP} \quad i \in 2, \dots, f - 1 \quad (5.4)$$

For MVR with vapor streams at stages in the rectifying section, the compressor outlet pressure can be calculated as shown in Eq. (5.5)

$$T_{N,HP} = T_{i,LP}(P_{N,HP}/P_{i,LP})^{(\gamma-1)/\gamma} \quad i \in 2, \dots, f - 1 \quad (5.5)$$

where $P_{i,LP}$ is the low pressure at stage i . By combining Eqs. (5.2), (5.4), and (5.5), it can be demonstrated that $P_{i,LP} > P_{1,LP}$.

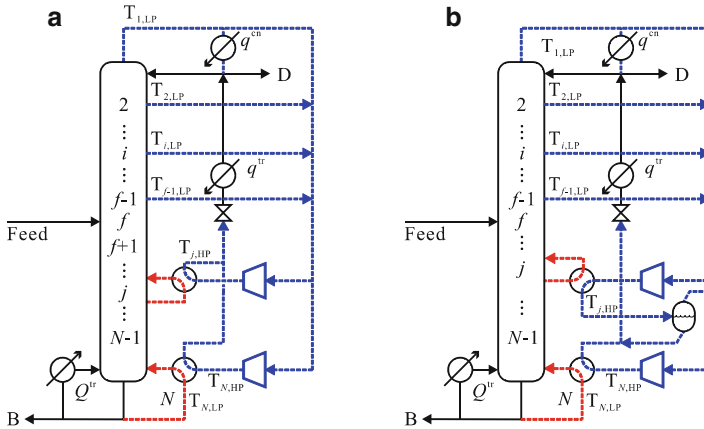


Fig. 5.9 Two-stage vapor recompression with heat-integrated stages. (a) Parallel. (b) series

Table 5.1 Simulation conditions for the n-heptane/benzene separation

Feed molar flow (kmol/h)	100
Feed composition n-heptane/benzene (mol%)	50/50
Feed condition	Saturated liquid
Condenser pressure (kPa)	100
Product purity n-heptane/benzene (mol%)	99.9/99.9

Therefore, the relations in Eqs. (5.6) and (5.7) can be derived

$$T_{N,HP} > T_{j,HP} > T_{i,LP} > T_{1,LP} \quad i \in 2, \dots, f - 1, \quad j \in f + 1, \dots, N - 1 \quad (5.6)$$

$$P_{N,HP} > P_{j,HP} > P_{i,LP} > P_{1,LP} \quad i \in 2, \dots, f - 1, \quad j \in f + 1, \dots, N - 1 \quad (5.7)$$

In addition to the feasible combinations for heat integration, the total work duty can be distributed in two or more compressors. This alternative is called in this chapter multistage mechanical vapor recompression. Figure 5.9 shows the possibilities to set two compressors in parallel (Fig. 5.9a) and in series (Fig. 5.9b).

Heat-integrated stages result in changes in condenser and reboiler heat duty reduction (Sect. 5.1.2.2) and the column temperature profile (Sect. 5.1.2.3); therefore, the best designs for MVR and MVR with heat-integrated stages are different. Table 5.1 shows the simulation conditions for the separation of an n-heptane/benzene mixture.

Simulations were done for this case study in Aspen Plus V8.0 by using the block RadFrac. Sensitivity analysis was done by varying the total number of stages (N), feed stage (FS) and heat-integrated stage locations (j) for MVR and MVR with heat-integrated stages. The simulation results were compared for the best design in terms of energy requirement (ER) and total annual cost (TAC) according to Eqs. (5.8) and (5.9)

Table 5.2 Additional parameters to calculate the TAC

Parameter	Value
Cooling water cost (\$/MWh)	0.86
Steam cost (\$/MWh)	45.4
Electricity cost (\$/MWh)	60.0
Cooling water temperature inlet/outlet (°C)	20/40
Steam temperature (°C)	147.6
Overall heat transfer coefficient condenser/reboiler/exchanger (kW/m ² K)	0.7/1.0/0.7
Compressor efficiency (–)	0.7
ΔT_{\min} (°C)	10.0

$$ER = Q^{tr} + \eta \sum_{k \in \text{COMP}} W_k \quad (5.8)$$

$$TAC = \frac{EC}{\theta} + \varphi OC \quad (5.9)$$

where η is the primary energy equivalent of electricity generation, θ is the payback time in years, and φ is the annual operation time in hours. W_k is the work duty of a compressor k , and COMP is the set of all compressors. EC is the equipment cost that comprises the column, trays, heat exchangers, and compressors cost and OC is the operation cost that comprises cooling water, steam, and electricity. The TAC was calculated according to the Guthrie method [10]. Note that η is a parameter that converts second energy sources (i.e., electricity generation) into primary energy sources (i.e., steam generation). The International Energy Agency estimates the primary energy equivalent from the electricity generation by assuming an efficiency of 33 % ($\eta = 1/0.33 = 3.03$), which is the average of nuclear power plants in Europe [11]. According to the Japanese Ministry of Economy, Trade, and Industry [12], the electricity generation efficiency in Japan is around 41 %, and the world average is 35 % ($\eta = 2.44$, and $\eta = 2.86$), respectively. Table 5.2 shows additional parameters to calculate EC and OC in Eq. (5.9).

Figure 5.10 shows the energy requirements for the simulation conditions in Table 5.1. The results show that MVR with heat-integrated stages require less energy than conventional MVR at conditions close to the minimum reflux ratio ($N = 100$), which agree with a previous work [13]. Furthermore, similar energy savings can be obtained at minimum reflux conditions regarding the stage subject to heat integration.

As the total number of stages decreases (higher reflux operation), the energy requirement for MVR with heat-integrated stages increases at a rate higher than that in conventional MVR up to the point that the latter is the best option ($N = 40$). In addition, as the stage subject to heat integration is set further from the reboiler, the increase rate of ER becomes higher ($i = N - 10$).

Figure 5.11 shows the simulation results when TAC is minimized for each given value of N . It shows that MVR with heat-integrated stages ($i = N - 2$) is economically better than conventional MVR for columns over 70 total stages ($N > 70$). This

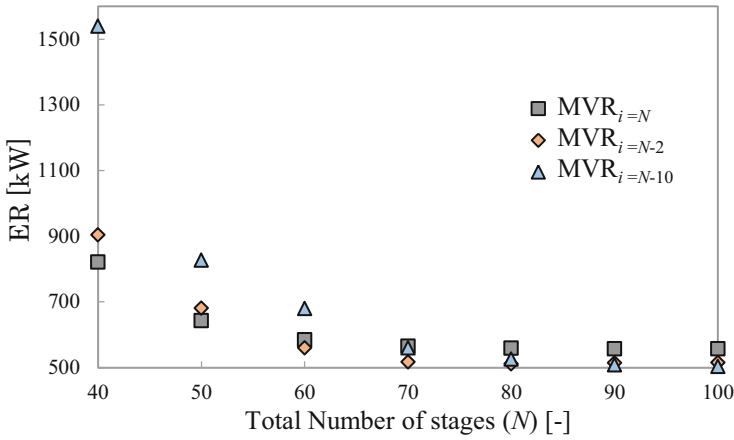


Fig. 5.10 Energy minimization for MVR and MVR with heat-integrated stages for the n-heptane/ benzene separation

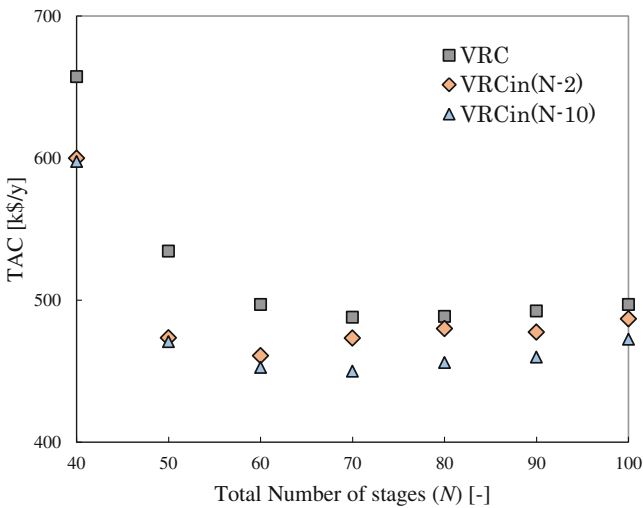


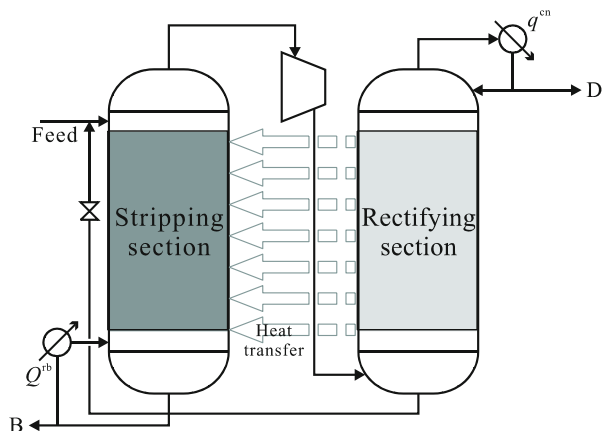
Fig. 5.11 TAC minimization for MVR and MVR with heat-integrated stages for the n-heptane/ benzene separation

cost reduction resulted from the reduction of electricity requirements and compressor size.

The comparison between MVR and MVR with heat-integrated stages for the presented separation of an n-heptane/benzene mixture showed that the latter can attain ER reduction around 10 % when the column operates near the minimum reflux ratio, but the ER reduction is less in columns at higher reflux ratio conditions.

For the results in Figs. 5.10 and 5.11, the optimization variable is the top vapor flow rate that enters the compressor. The relation between vapor flow rate and

Fig. 5.12 Conceptual HIDiC representation



pressure change is very important to obtain the best heat exchange between the upgraded heat of the vapor leaving the condenser and a stage subject to heat integration.

5.3.2 Heat-Integrated Distillation Column

The HIDiC is an intensified distillation column that involves internal heat integration between the whole rectifying and the whole stripping sections, and it is also another kind of heat-pump distillation column. Although the idea that actually included internal heat integration between part of the rectifying and the stripping sections was conceived in the late 1970s [14], it was not until 1990s that the importance of internal heat integration gained interest, and it was demonstrated that it plays an important role in energy efficiency for a given separation. Therefore, the idea of internal heat integration was extended to realize heat integration in the whole rectifying and the whole stripping sections. Because HIDiC offers several attractive features, its industrialization in chemical and petrochemical process industries has been encouraged. These features include mainly [15]:

1. Energy efficiency higher than that in conventional distillation columns.
2. In the ideal case, zero external reflux and reboil flows.

Figure 5.12 shows the conceptual representation of a HIDiC, which has been used to find the heat loads at all stages in the column. In addition, the design, simulation, and optimization results of HIDiC show that it can attain energy savings more than 50 %, economic savings, and reduction in the entropy production for the separation of binary mixtures and ternary mixtures [16–31].

Although Fig. 5.12 has been used as conceptual representation for simulation and optimization purposes, the construction can be either done by using two concentric tubes arrangement with different tube circumferences (Fig. 5.13) or

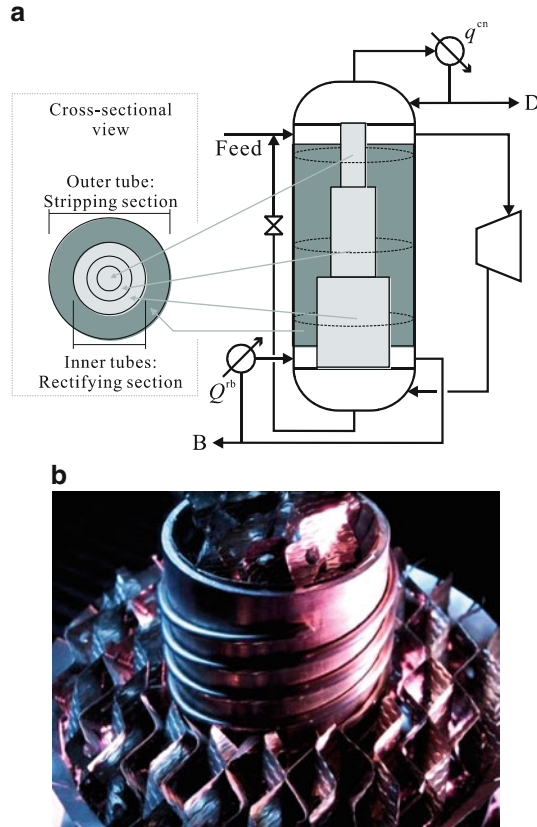


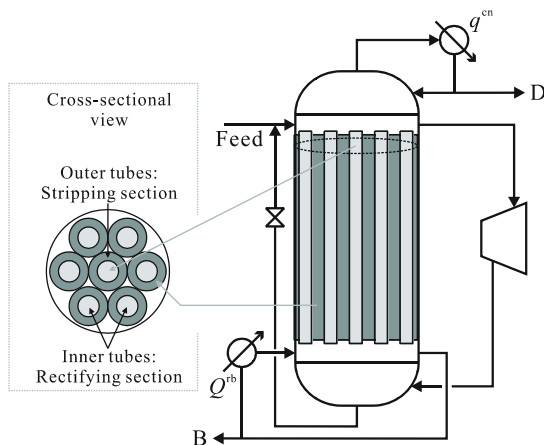
Fig. 5.13 HIDiC design with inner tubes of different diameter. (a) conceptual representation. (b) practical implementation (Source: Kimura Chemical Plants Co., Ltd. in website of New Energy and Industrial Technology Development Organization (NEDO). <http://www.nedo.go.jp/hyoukabu/articles/201214kcpc/index.html> Accessed 24 Feb 2015)

multiple tubes arrangement in which the rectifying section is in the inner tubes while the stripping section is in the outer tubes (Fig. 5.14).

In Fig. 5.13a, the inner tubes make the rectifying section (lighter solid area) while the outer tubes make the stripping section (darker solid area). It also can be seeing that the cross-sectional area decreases towards the bottom in the stripping section and towards the top in the rectifying section. The diameter of the rectifying section gradually decreases for the ideal case [18] and segmentally for a more practical case [19, 20]. Figure 5.13b shows the actual equipment of a concentric HIDiC. The inner part is the rectifying section and the outer part is the stripping section.

The HIDiC configuration in Fig. 5.14 has multiple concentric cylinders. Similarly, the inner tubes make the rectifying section (lighter solid area) while the outer tubes make the stripping section (darker solid area). Also the cross-sectional area

Fig. 5.14 HIDiC design with multiple concentric tubes



decreases towards the bottom in the stripping section and towards the top in the rectifying section, but the changes in diameter are small. This configuration has been implemented at a pilot plant scale [22].

The selection of the best configuration is case specific because for the separation of some mixtures, the constant heat distribution with variable heat transfer area is better than the constant heat transfer area with variable heat load [18].

5.3.3 HIDiC with Fewer Heat-Integrated Stages

Typically in HIDiC, heat integration takes place along the whole rectifying and stripping sections, which can raise maintenance issues due to blockage in the column internals (trays or packing) because of deposition of solid particles in mixtures containing suspended solids (e.g., pigments, catalysts, ashes), monomers which can undergo polymerization or solidification reactions, and salts (e.g., calcium sulfate) which can produce crystals that can also deposit in the heat transfer surface [24].

In addition, the operability and controllability of HIDiC are other important issues. The complex heat integration structure of HIDiC might make its operation more difficult than conventional distillation columns because HIDiC can require more complex PID control configurations [25], it can be more sensitive to the system disturbances [26], and it can have multiple steady states depending on the heat load distribution changes along the column during operation [27].

Because of the aforementioned issues in typical HIDiC, its implementation in chemical and petrochemical plants has not been realized. However, the reduction of the number of heat-integrated stages can alleviate maintenance and operability issues while attaining high energy savings. The configurations with less heat-integrated stages have been proven to be better than fully integrated

Table 5.3 Effect of the number of side heat exchangers for the benzene/toluene mixture [29]

Feed molar flow benzene/toluene (kmol/h)	50/50		
Liquid molar fraction in the feed (%)	50		
Product purity benzene/toluene (mol%)	99.9/99.9		
Stages in the rectifying section (M) (-)	15		
Stages in the stripping section (N) (-)	18		
Rectifying section pressure (kPa)	101.3		
Number of side heat exchangers	3	4	5
Total amount of heat exchanged (kW)	1412	1586	1570
Total heat transfer area (m ²)	393	350	399
Rectifying section pressure (kPa)	225	212	213
Combinations of side heat exchanges (i, j) (-) $i \in 1, \dots, M$ $j \in 1, \dots, N$	1,3	1,1	1,1
	12,17	8,4	6,4
	15,18	14,17	13,11
		15,18	14,17
			15,18

HIDiC through the solution of optimization techniques and numerical analysis [3, 17, 28, 29].

The optimal heat distribution at stages in HIDiC is crucial for developing a column with a simpler structure. The heat distribution at each column section can be determined by the temperature difference profile between the rectifying section and the stripping section. In addition, the effect of internal heat integration on the reduction of reboiler heat load depends strongly on the location of heat exchange stages [28]. Table 5.3 shows the simulation conditions to design a HIDiC with few heat-integrated stages for the separation of a benzene/toluene mixture. The total heat transfer area of side heat exchangers becomes minimum when the number of side heat exchangers is four as shown in Fig. 5.15. The optimal number of heat integrations is case specific, and it largely depends on the shape of the reversible distillation curve for the given mixture.

5.3.3.1 Comparison Between MVR and HIDiC

Although several works have compared MVR and HIDiC schemes in terms of energy and economic savings, the results are not conclusive to consider one over the other. In fact, the selection of each technology is case specific. As confirmed in many research works [5–8, 13–22, 30, 31], MVR and HIDiC result in lower energy requirements and operation cost; however, they usually have higher equipment cost. Therefore, in some cases, the increase in equipment cost can overtake the reduction in operation cost [23]. Finally, the comparison between MVR, VC, and HIDiC has not considered heat pump systems with heat-integrated stages

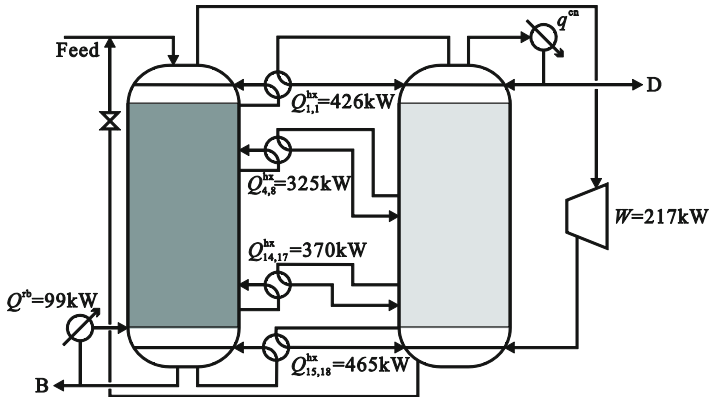


Fig. 5.15 HIDiC design with shifted rectifying and stripping sections [29]

(Sect. 5.3.1) or HIDiC with fewer heat-integrated stages (Sect. 5.3.3). These comparisons remain as open questions that must be assessed from the conceptual level to the final implementation.

5.4 Heat Integration Through Side Heat Exchangers

In addition to heat pump systems, there are other intensified distillation processes that avoid using a compressor. As seen in the previous section, a compressor is used to upgrade the heat of vapor streams; however, another way is by using the heat of vapor streams from other columns or processes to realize heat integration at stages. External heat integration (also known as multiple effect distillation, or multi-effect distillation) has been widely used as energy conservation method in which the condenser of a high-pressure column supplies heat to the reboiler of a low-pressure column. In this section, the concept of multi-effect distillation is extended to consider heat-integrated stages as an option for intensification of distillation columns.

5.4.1 Compressor-Free HIDiC

Although the potential high energy saving of HIDiC has been recognized, there are not commercial-scale HIDiC implementations. One reason is because petrochemical companies have plenty of steam from the direct cracking process which releases high cascade heat [24]. Another problem is that a big compressor with large discharge rate has to be installed. Finally, HIDiC is not suitable for the separation of mixtures with solid suspended particles (see Sect. 5.3.3).

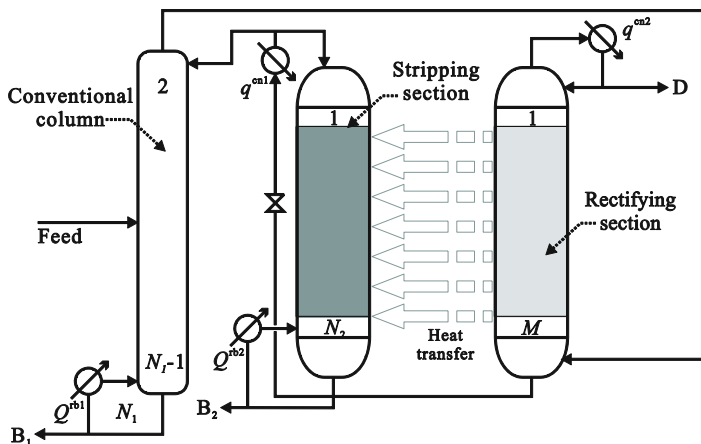


Fig. 5.16 Conceptual representation of a compressor-free HIDiC

To avoid the use of a compressor, a compressor-free HIDiC (CF-HIDiC) has been proposed [24, 32–34]. It has been studied to enrich bioethanol from diluted mixture [30], to recover solvents in wastewater streams [33], and to separate a benzene/toluene mixture [34]. Figure 5.16 shows a conceptual representation of a CF-HIDiC. The feed is supplied to a conventional column at high pressure, and its top vapor stream is fed to the rectifying section of the HIDiC column, then the liquid leaving the rectifying section enters the top of the stripping section of the HIDiC column. It can be seen that the compressor is replaced by an additional column that supplies vapor streams at high pressure. In the case of ethanol enriching, the operation at high pressure results in serious fouling because the deposition of solid components, therefore vacuum conditions in the stripping section can be enforced to avoid fouling. Thus, the conventional column and the rectifying section can operate at atmospheric pressure.

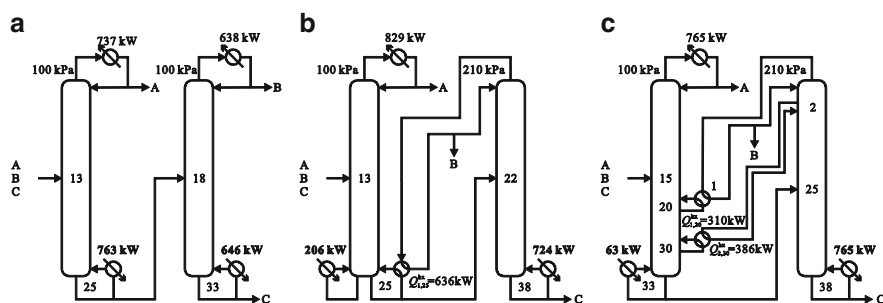
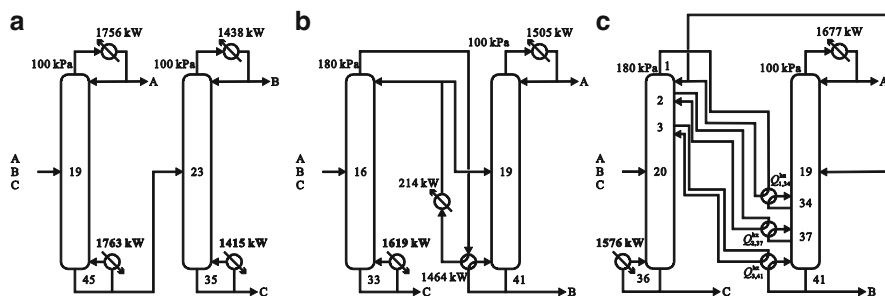
5.4.2 Externally and Internally Heat-Integrated Distillation

Heat-integrated stages by means of side heat exchangers have been proposed to separate binary mixtures of close boiling points [35], the separation of ternary [1, 2, 36, 37], and multicomponent mixtures [38]. However, as the number of components in the mixtures increases, the number of possible distillation sequences increases and the heat integration possibilities for all sequences enormously increase. Therefore, most of the simulation, optimization, and design approaches have been limited to two distillation columns.

Table 5.4 shows the simulation conditions for the separation of two ternary mixtures, in which the conventional, externally heat-integrated sequence (multi-effect distillation), and internally heat-integrated sequence are compared.

Table 5.4 Simulation conditions for ternary mixtures

	Case 1	Case 2
Mixture	Cyclopentane (A)/benzene (B)/toluene (C)	Methanol (A)/ethanol (B)/propanol (C)
Feed molar flow (kmol/h)	100	100
Feed composition (A/B/C) (mol%)	40/30/30	25/50/25
Product purity (A/B/C) (mol%)	98/98/98	99/99/99
Feed condition	Saturated liquid	Saturated liquid
Low-pressure column (LPC) (kPa)	100	100
High-pressure column (HPC) (kPa)	Variable	Variable

**Fig. 5.17** Solutions for case 1. (a) Conventional. (b) Multi-effect. (c) Heat-integrated stages**Fig. 5.18** Solutions for case 2. (a) Conventional. (b) Multi-effect. (c) Heat-integrated stages

Figures 5.17 and 5.18 show the results for the mixtures in Table 5.4. For the separation in case 1, the best option is the direct distillation sequence in all cases while for the separation in case 2, the best option is the indirect distillation sequence in all cases. The energy saving for heat-integrated stages is higher than the typical multi-effect distillation for both cases.

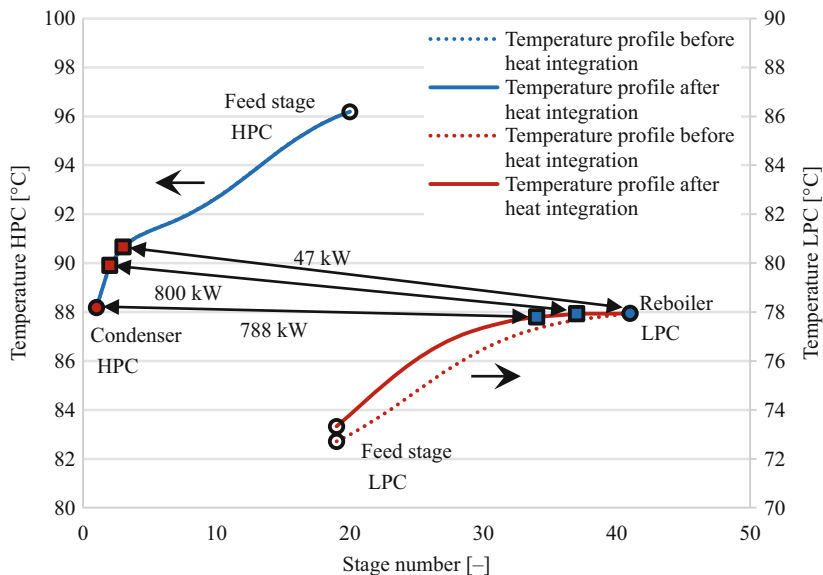


Fig. 5.19 Changes in the temperature profile for case 2 with heat-integrated stages

Each alternative is optimized individually in Figs. 5.17 and 5.18. The trim reboiler heat duty in Fig. 5.17b can be reduced by increasing the heat exchange between columns. Although the total amount of heat exchanged in Fig. 5.17c (696 kW) is higher than that in Fig. 5.17b (636 kW), the temperature difference in the former is also higher than that in the latter; therefore, the total heat transfer area and the exchangers cost will not largely change between Fig. 5.17b, c.

In Fig. 5.18, heat integration between stages can be used to eliminate the trim condenser by supplying heat from stage 1 in the HPC to stage 34 in the LPC. The total amount of heat exchanged in Fig. 5.18c (1635 kW) is higher than that in Fig. 5.18b (1464 kW); however, the temperature difference in the former is also higher than that in the latter; therefore, the total heat transfer area and the exchangers cost will not largely change between Fig. 5.18b, c.

Figure 5.19 shows the changes in the temperature profile in the rectifying section of the HPC and the stripping section of the LPC for case 2 in Table 5.4. When heat integration is done at stages close to the condenser, there are almost no changes in its temperature profile. Contrarily, when heat integration is done at stages far from the reboiler, there are changes in its temperature profile. These changes in the temperature profile, amount of heat exchanged, and heat transfer area must be considered and solved simultaneously at the simulation and optimization of intensified heat-integrated distillation.

5.5 Heat-Integrated Distillation Involving Reactive Systems

By combining two important operations (reaction and separation) into a single vessel, reactive distillation has demonstrated its potential for capital productivity improvements, selectivity improvements, reduced energy use, and the reduction or elimination of solvents in the process. Some reviews about reactive distillation have been done and a total of 562 publications of reactive distillation for the period of 1971–1999 [39], 1105 publications and 814 US patents between 1971 and 2007 [40], and over one hundred industrially or potentially important reactions for reactive distillation applications [41] have been studied. This shows the rapid progress of this technology in recent years, and its importance in industrial applications.

For exothermic reaction systems utilizing reactive distillation, the operating energy can be reduced by making use of this heat of reactions to partially supply vapor traffic inside the column. However, many endothermic reaction systems can still benefit from the reactive distillation technology for conversion and selectivity improvements. For these endothermic reaction systems, operating the reactive distillation column at higher pressure (which means the system is operated at higher temperature condition) would benefit from the shifting of the reaction to the product side. Moreover, heat integration methods via pressurized operation in the open literature can be utilized to further save energy of these reactive distillation systems.

In the following subsections, reactive thermally coupled and reactive multi-effect will be addressed for the hydrolysis of methyl acetate and esterification of isopropyl alcohol.

5.5.1 Hydrolysis of Methyl Acetate Reactive Distillation Process

In a polyvinyl alcohol (PVA) plant shown in Fig. 5.20, reaction stoichiometry indicates that equal moles of methyl acetate are generated for every mole of PVA produced. One way to convert methyl acetate back to acetic acid (the raw material of PVA plant) is via methyl acetate hydrolysis. The best design of a reactive

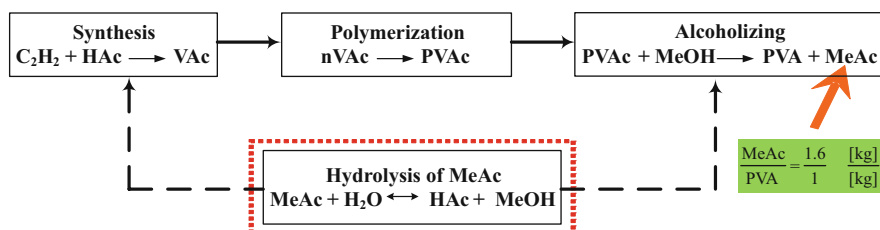


Fig. 5.20 Polyvinyl alcohol production process block diagram

distillation process has been proposed by Lin and his coworkers [42, 43]. The design of this process for exploring the reactive HiDiC and reactive multi-effect of heat-integration in a reactive distillation system with methyl acetate hydrolysis reaction was studied by Lee et al. [44]. From their work, reactive multi-effect is a better configuration than the arrangement of reactive HiDiC. For understanding the reactive multi-effect, the design of this arrangement will be introduced in the following subsections. Moreover, the thermally coupled configuration of this process will be studied to demonstrate the result of energy saving for these two kinds of heat-integrated methods.

5.5.1.1 Reaction Kinetics and Phase Equilibrium

There are four components in the methyl acetate hydrolysis process including two reactants: methyl acetate (MeAc) and water (H₂O); and two products: acetic acid (HAc) and methanol (MeOH). The endothermic reversible reaction of this process is shown below:



Two kinetic model forms (pseudo-homogeneous and adsorption based) were used to fit the experimental data, and the used heterogeneous catalyst was Amberlyst[®] 15 [45, 46]. It was found that the adsorption-based model fits the experimental data better. Table 5.5 shows the kinetic model based on activity. M_i [kg/kmol] is the molecular weight of component i and R (8.314 kJ/kmol/K) is the gas constant. Notice that the unit of the reaction constants is in kmol/kg_{cat}/s which will be converted to kmol/m³/s in the simulation study with the assumption of catalyst density at 770 kg/m³ and catalyst occupied half of the liquid holdup in the reactive tray.

The equilibrium constants ($K_{\text{eq}} = k_f/k_r$) calculated at two different temperatures are also listed in Table 5.5. Since the value of the equilibrium constant is small, excess water design has been conducted in order to drive methyl acetate to near

Table 5.5 Kinetic model and parameters for the studied system

Kinetic model (catalyst)	k_f	K_{eq}
Adsorption-based model (Amberlyst [®] 15)	At $T = 333$ K $k_f = 1.01 \times 10^{-6}$ [kmol/kg _{cat} /s]	At $T = 333$ K $K_{\text{eq}} = 0.039$
$r = m_{\text{cat}} \cdot \frac{k_f a_{\text{MeAc}} a_{\text{H}_2\text{O}} - k_r a_{\text{HAc}} a_{\text{MeOH}}}{\left(a'_{\text{MeAc}} + a'_{\text{H}_2\text{O}} + a'_{\text{HAc}} + a'_{\text{MeOH}}\right)^2}$ $a'_i = \frac{K_i a_i}{M_i}, K_{\text{MeAc}} = 4.15, K_{\text{H}_2\text{O}} = 5.24, K_{\text{HAc}} = 3.15,$ $K_{\text{MeOH}} = 5.64$		
$k_f = 1.000 \times 10^4 \exp\left(\frac{-63,730}{RT}\right)$ $k_r = 7.862 \times 10^4 \exp\left(\frac{-60,470}{RT}\right)$ $\Delta H = 3260 \text{ (kJ/kmol)}$	At $T = 393$ K k_f $= 3.38 \times 10^{-5}$ (kmol/ kg _{cat} /s)	At $T = 393$ K $K_{\text{eq}} = 0.046$

complete conversion [42, 43]. Because the reaction is endothermic, the calculated equilibrium constant is more favorable at higher operating temperature ($K_{\text{eq}} = 0.046$ at 393 K against $K_{\text{eq}} = 0.039$ at 333 K). However, there is an upper limit on the operating temperature for Amberlyst[®] 15 at 120 °C. This information was used later to set the pressure upper limit in order to achieve heat-integration in the process.

The UNIQUAC model was used to calculate the liquid activity coefficient and Hayden and O'Connell (HOC) model was used to account for association in the vapor phase [47]. The parameters for the UNIQUAC model are listed in Table 5.6.

5.5.1.2 Base Design Flowsheet of the Overall Process

There are two azeotropes in the studied system. The boiling point ranking of the four components, as well as the two azeotropes, is shown in Table 5.7. It is found that although one product (HAc) is the heaviest boiling point component, the other product (MeOH) is in the second lightest boiling point component. Thus, it is more difficult to come up with the overall design flowsheet in Fig. 5.21 [43].

In Fig. 5.21, the flowsheet includes a reactive distillation column and two other columns. The two fresh feed streams enter into the reflux drum of the reactive distillation column, which is under total reflux operation and the reaction section is

Table 5.6 UNIQUAC model parameters for the methyl acetate hydrolysis

(i,j)	a_{ij} (K)	a_{ji} (K)	b_{ij} (K)	b_{ji} (K)	c_{ij} (K ⁻¹)	c_{ji} (K ⁻¹)
(1,2)	-0.9704	2.0346	-390.26	-65.245	0.003061	-0.003157
(1,3)	0.4364	-1.1162	62.19	-81.848	-0.0002724	0.001331
(1,4)	0.05101	0.2936	-422.38	98.120	0.0002402	0.00007674
(2,3)	0.7101	-0.7248	-62.97	-326.20	-0.001167	0.002355
(2,4)	-3.1453	2.0585	575.68	-219.04	0.006071	-0.007015
(3,4)	-0.01014	-0.9630	-593.70	265.83	0.002161	-0.0002013

1: HAc; 2: MeOH; 3: MeAc; 4: H₂O

Table 5.7 Boiling point ranking at 1 and 4.6 atm

Components boiling point ranking (from low to high)	1 atm	4.6 atm
MeAc/MeOH	53.65 °C (0.653/0.347)	101.73 °C (0.51/0.49)
MeAc/H ₂ O	56.43 °C (0.89/0.11)	106.16 °C (0.78/0.22)
MeAc	57.05 °C	109.00 °C
MeOH	64.53 °C	109.14 °C
H ₂ O	100.02 °C	149.29 °C
HAc	118.01 °C	175.92 °C

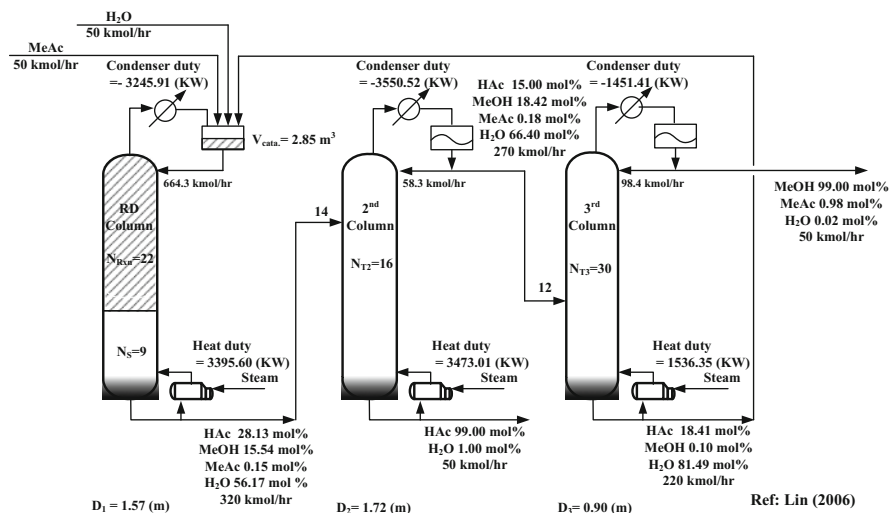


Fig. 5.21 Base design for the methyl acetate hydrolysis process using reactive distillation [43]

at the upper part of the column. All products and unreacted components are withdrawn from the bottom of the column and fed downstream to the separation system consisting of two columns. Since there is negligible methyl acetate in this feed stream to the downstream system, the separation should be easy because there is not an azeotrope in the ternary system of acetic acid, water, and methanol. The first column in the separation system separates acetic acid (heavy product) at the bottom, and the second column separates methanol (light product) at the top. The bottom of the second column is designed to avoid tangent pinch at the pure water end; thus, it contains mostly water with some acetic acid. The water-rich stream is recycled back to the reactive distillation column. The overall design shown in Fig. 5.21 corresponds to the minimum TAC. An extended design flowsheet with a mixed feed of MeAc and MeOH instead of pure MeAc feed has been also proposed, which used a similar design concept [42].

In Fig. 5.21, the indirect sequence (heaviest out first) was used for the design of the separation system. Heat integration of this separation system is possible by using a pre-fractionator column and a main column with side draw, a Petlyuk column, or a column with dividing wall.

5.5.2 Isopropyl Acetate Reactive Distillation Process

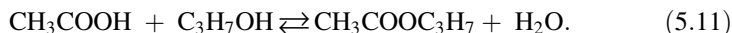
Another case is the esterification of isopropyl alcohol to produce isopropyl acetate (IPAc). Different process flowsheets for the esterification of acetic acid with C1-C5 alcohols have been developed [48]. These flowsheets show that high-purity ester

products can be produced using reactive distillation technology. Furthermore, it was demonstrated that industrial quality ethyl acetate product can be obtained in a pilot plant test [49] by using the flowsheet [48].

Lee et al. [50] had proposed an interesting flowsheet for the heat integration through a thermally coupled arrangement. Unlike the conventional heat-integrated process, the combination of a reactive distillation and a decanter to split the organic and aqueous phases can be intensified by using a thermally coupled arrangement (see Sect. 5.5.3.2). Furthermore, reactive multi-effect distillation for this process will be also studied (see Sect. 5.5.4.2).

5.5.2.1 Reaction Kinetics and Phase Equilibrium

By reacting isopropanol (IPOH) with acetic acid (HAc), the esterification reaction will produce isopropyl acetate (IPAc) and water (H₂O). The reactions are reversible and the stoichiometric balance equation is shown below:



The used solid catalyst is the acidic ion-exchange resin of Amberlyst[®] 15. Table 5.8 displays the reaction rates expressed in the Langmuir-Hinshelwood model form. Notice that the kinetic model is represented in terms of activity and the reaction is catalyst-weight (m_{cat}) based. The catalyst-weight is computed by assuming that the solid catalyst occupies 50 % of the tray holdup and a catalyst density of 770 kg/m³ is used to convert the volume into catalyst-weight. A FORTRAN subroutine is written in Aspen Plus to compute the extent of reaction at each reactive tray.

The isopropyl acetate process exhibits nonideal phase behavior and has four azeotropes. In order to accurately represent the phase equilibria of the process, it is essential to select a reliable thermodynamic model. To account for the nonideal vapor–liquid equilibrium (VLE) and vapor–liquid–liquid equilibrium (VLLE) for the quaternary system, the NRTL (non-random two-liquid) activity coefficient

Table 5.8 Kinetic equations for IPAc processes

Kinetic model (catalyst)	k_1 ($T = 363$ K)	K_{eq} ($T = 363$ K)
Langmuir-Hinshelwood/Hougen-Watson model (Amberlyst 15 by Gadewar et al. [51])	2.26×10^{-4} (kmol/(kg _{cat} s))	8.7
$r = m_{\text{cat}} \frac{k_1 (a_{\text{HAc}} a_{\text{IPOH}} - a_{\text{IPAc}} a_{\text{H}_2\text{O}} / K_{\text{eq}})}{(1 + K_{\text{HAc}} a_{\text{HAc}} + K_{\text{IPOH}} a_{\text{IPOH}} + K_{\text{IPAc}} a_{\text{IPAc}} + K_{\text{H}_2\text{O}} a_{\text{H}_2\text{O}})^2}$		
$k_1 = 7.667 \times 10^{-5} \exp(23.81 - \frac{68,620.43}{RT})$		
$K_{\text{eq}} = 8.7, K_{\text{HAc}} = 0.1976, K_{\text{IPOH}} = 0.2396, K_{\text{IPAc}} = 0.147,$ $K_{\text{H}_2\text{O}} = 0.5079$		
Assumption: mol H ⁺ /kg _{cat} = 4.6×10^{-3}		

$R = 8.314$ (kJ/k mol/K), T (K), r (k mol/s), m_{cat} (kg_{cat}), x_i (mole fraction)

Table 5.9 The NRTL model coefficients for IPAc process

Comp. i	HAc	HAc	HAc	IPOH	IPOH	IPAc
Comp. j	IPOH	IPAc	H ₂ O	IPAc	H ₂ O	H ₂ O
b_{ij} (K)	-141.644	70.965	-110.580	191.086	20.057	415.478
b_{ji} (K)	40.962	77.900	424.060	157.103	833.042	1373.462
c_{ij}	0.305	0.301	0.299	0.3	0.325	0.3

Table 5.10 The compositions and temperatures of the azeotropes for IPAc process

Comp. i	Experimental components	Experimental Temp. (°C)	Computed components	Computed Temp. (°C)
IPOH-IPAc	(0.6508,0.3492)	80.1	(0.5984,0.4016)	78.54
IPOH-H ₂ O	(0.6875,0.3125)	82.5	(0.6691,0.3309)	80.06
IPAc-H₂O	(0.5982,0.4018)	76.6	(0.5981,0.4019)	76.57
IPOH-IPAc-H₂O	(0.1377,0.4938,0.3885)	75.5	(0.2377,0.4092,0.3531)	74.22

Heterogeneous azeotropes are in boldface. Experimental data from Horsley [56]

model is adopted in Aspen Plus. The NRTL model parameter sets shown in Table 5.9 are taken from Tang et al. [48]. The vapor phase non-ideality such as the dimerization of acetic acid is also considered. The second virial coefficients of Hayden-O'Connell [47] are used to account for vapor phase association of acetic acid. The Aspen Plus built-in association parameters are used to compute the fugacity coefficients.

The thermodynamic model predicts three binary minimum boiling azeotropes and one ternary minimum boiling azeotrope [48]. Table 5.10 shows that the model prediction results of the azeotropes temperatures and compositions are in good agreement with the experimental data. Notice that the lowest temperature of the system is at the ternary minimum boiling azeotrope. This ternary azeotrope is shown in the residue curve map (RCM) in Fig. 5.22.

5.5.3 Thermally Coupled Configurations with Reactive Systems

The hydrolysis of methyl acetate and esterification of isopropyl alcohol are taken up as case studies to demonstrate the feasibility of thermally coupled configurations with reactive systems.

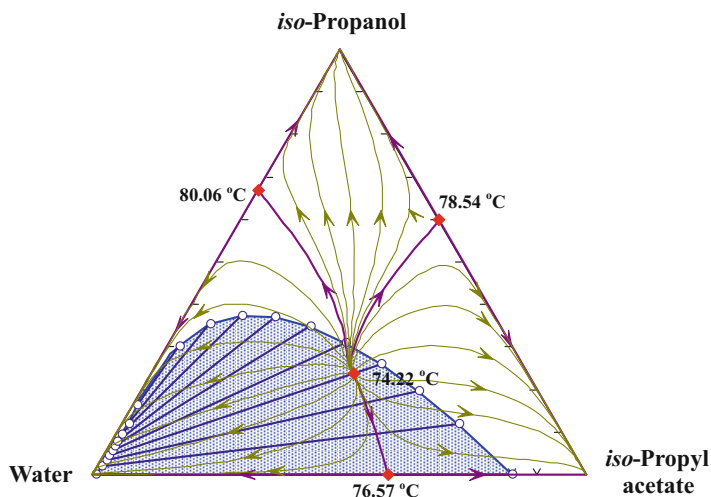
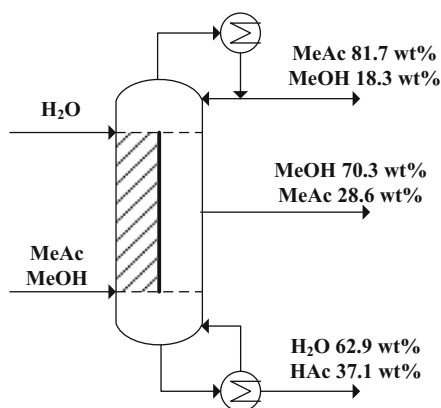


Fig. 5.22 Ternary RCMs and LLEs of IPAc process

Fig. 5.23 The first study of an RDWC for the hydrolysis of methyl acetate [52]



5.5.3.1 Thermally Coupled Process for the Hydrolysis of Methyl Acetate

For the hydrolysis of methyl acetate, Sander et al. [52] had established that the operation of a reactive divided wall column (which called RDWC) is possible; however, the results in Fig. 5.23 show that the purity of products and the desired methyl acetate conversion are not good [52].

To achieve the industrial product specifications, an RD column with a reactive reflux drum and two separation columns have been proposed in Lin's work [42, 43]. The advantages of DWC are combined with the hydrolysis of methyl acetate RD and propose a better thermally coupled configuration (see Sect. 5.5.1.1

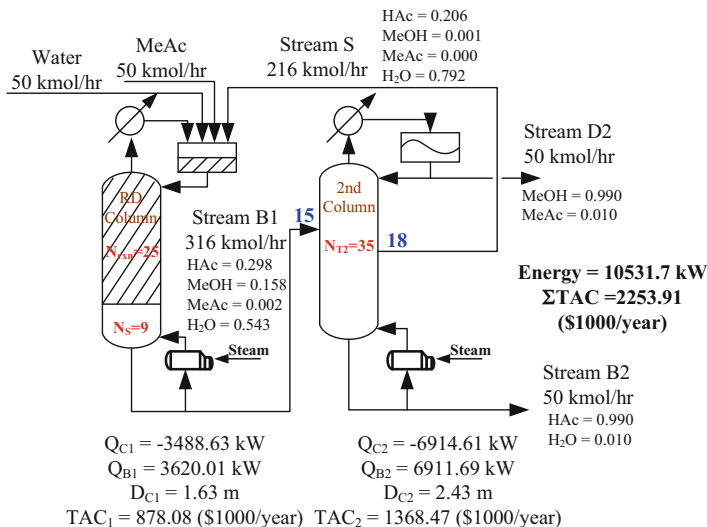


Fig. 5.24 RD with a sidedraw column

for the thermodynamic and kinetic data). The objective function is to minimize TAC, see Eq. (5.9), with a payback of 3 years ($\theta=3$). The equipment cost comprises the costs of the column, trays, and heat exchangers and they are calculated according to Douglas's textbook [53].

The prototype of thermally coupled configuration comes from the RD with a side draw column, which is shown in Fig. 5.24. This configuration has one RD column and one additional column to separate MeOH and HAc at the top and bottom, respectively. The sidedraw stream which is rich in water recycles back to the RD column reflux drum. The optimal design of RD with a sidedraw column in Fig. 5.24 has a TAC of 2253.91 (\$1000/year) and overall energy consumption of 10,531.7 kW.

The composition profiles of RD column are displayed in Fig. 5.25. Because of the small equilibrium constant, a large amount of water-rich stream is fed back to the RD reflux drum to attain complete conversion of the limiting reactant MeAc. The water-rich stream recycle causes the reactant's concentrations to improve the reaction rate of this second-order reaction near the reactive zone. Thus, HAc, MeOH, and water are the major obtained components at the RD column bottom. Although the MeOH reaches 0.40 composition at stage 30, it drops to 0.155 at the column bottom (i.e., stage 34). This phenomenon is the so-called remixing effect.

This configuration can meet the product specifications. Nevertheless, the TAC and energy consumption increased up to 25.3 and 23.5 % in comparison with the base design configuration. For the RD column, TAC and energy consumption increased 8.6 and 6.6 %. For the separation column, TAC and energy consumption increased 34.7 and 38 %. The previous results imply that the TAC and energy consumption in the separation column dominate the overall process TAC and

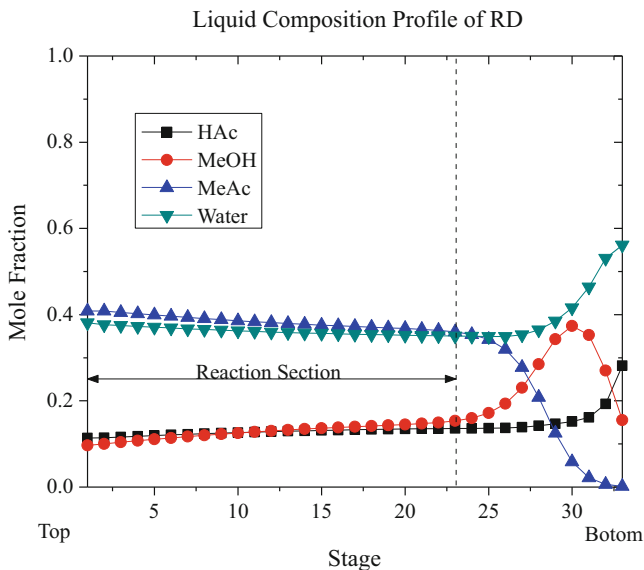


Fig. 5.25 Composition profiles of RD with a side draw column

energy consumption. According to the heuristics proposed by Tedder and Rudd [54] for ternary mixtures, the RD bottom compositions are unfavorable to be separated by a side draw column. This is why the energy consumption in the separation column is high.

Figure 5.26 shows a thermally coupled reactive distillation for the hydrolysis of methyl acetate, which is an alternative that can replace the design of RD with a sidedraw column. Because the liquid and vapor need to interact between RD and sidedraw column, the RD reboiler is removed and replaced by a sidedraw vapor stream from the second column. As a result, the sidedraw vapor stream location and its flow rate are additional design variables.

After the sequential iteration (see Sect. 5.2.2), Fig. 5.26 corresponds to the optimal thermally coupled reactive distillation result. The TAC is 1622.04 (\$1000/year) and its overall energy consumption is 5750 kW. Thermally coupled design of RD with a sidedraw column has a great improvement of 31.6 % energy savings and 11.1 % reduction of TAC (see Table 5.11). It can save 45.4 % energy consumption and 28 % TAC compared to RD with a sidedraw column. The use of thermal coupling demonstrates that intensification of RD processes leads to very significant savings in energy consumption, operating cost, and capital cost with a smaller column.

Figure 5.27 shows the RD composition profiles for the thermally coupled solution in Fig. 5.26. MeOH has the highest composition and MeAc has the lowest composition at the RD bottom of the thermally coupled RD configuration. The lightest product MeOH composition steadily increases up to 0.473 mol fraction in

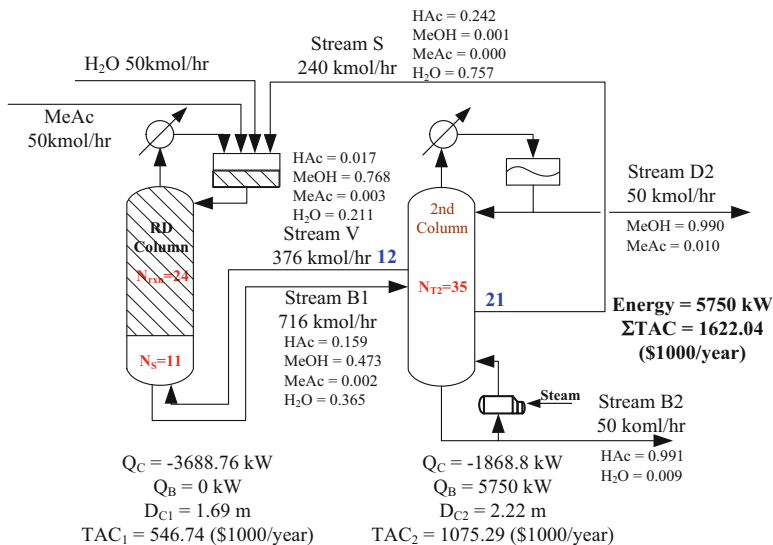


Fig. 5.26 Thermally coupled design of RD with a sidraw column

Table 5.11 TAC results and energy consumption comparison with conventional and thermally coupled configurations

	Energy (kW)	TAC (\$1000/year)	Energy saving (%)	TAC saving (%)
Base design [43]	8403.1	1824.48	—	—
RD with a sidraw column	10531.7	2253.91	-25.33	-23.54
RD with thermally coupled configuration	5750.0	1622.04	31.57	11.10

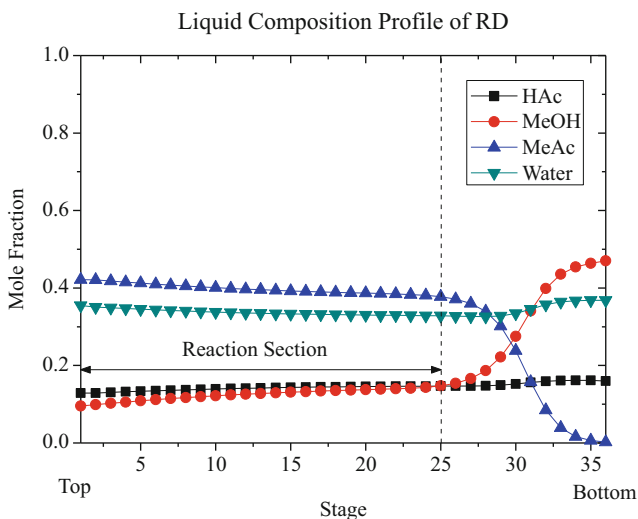


Fig. 5.27 RD composition profiles of the thermally coupled configuration

the RD bottom. In addition, the remixing effect (i.e., poor thermodynamic efficiency phenomenon) of the MeOH product composition disappears in the thermally coupled RD configuration. Thus, larger liquid flow rate with higher MeOH composition feeds the column with side draw. As a result, the MeOH composition is much higher, which would be helpful to attain energy savings.

5.5.3.2 Thermally Coupled Process for the Esterification of Isopropyl Alcohol

In this section, the advantages of reactive distillation with thermally coupled configuration for the esterification of isopropyl alcohol will be introduced based on the work of Lee et al. [50].

Based on the azeotrope and boiling point ranking, the heaviest component is the reactant HAc so that no bottom outlet stream of the RD column is designed. The top composition of the RD column is quite close to the minimum temperature azeotrope of IPOH-IPAc-H₂O. It is found in Fig. 5.22 that the liquid–liquid envelope (LLE) is quite large, and the ternary minimum boiling azeotrope lies well inside the envelope. It can also be seen that all the tie lines point towards the pure water end and, consequently, relatively pure water can be recovered from the aqueous phase in a decanter designed to be located at the top of the RD column. The tie lines can also pass across the distillation boundary so that high-purity IPAc can be obtained by further purification of the organic phase outlet stream in a stripper. Part of the organic phase material is also refluxed back to the RD column in order to withdraw water from the system. Due to economic reasons, the thermally coupled IPAc process configuration uses feed streams from industrial compositions of reactants instead of pure feed streams.

Figure 5.28 shows the optimal result of the conventional IPAc RD process [49]. The IPOH feed is assumed to be close to the azeotrope compositions. The HAc feed composition is set to be 95 mol% and that of IPOH is set to be 64.91 mol%, respectively. The product specifications include IPAc production with 99 mol% while keeping HAc purity below 0.01 mol%. The numbers of stages in the rectifying, reactive, and stripping sections are the same as in the study carried by Lai et al. [49].

Figure 5.29 shows the composition profiles of the IPAc process. The IPAc composition reaches its highest value at stage 3; then, it decreases towards the top of the RD column. This phenomenon is termed “remixing effect,” which hints that there is potential for energy saving by using thermally coupled configuration. Another observation is that the top compositions of the RD column and the stripper are quite close in Fig. 5.28, and these compositions are located into the LLE aqueous phase.

Figure 5.30 shows the thermally coupled RD configuration. Based on the solution in Fig. 5.28, the feed to the stripper is from the organic outlet stream of the decanter; therefore, it has been decided to place the decanter on the stripper. A liquid stream is needed to flow down to the RD column and to act as entrainer so as

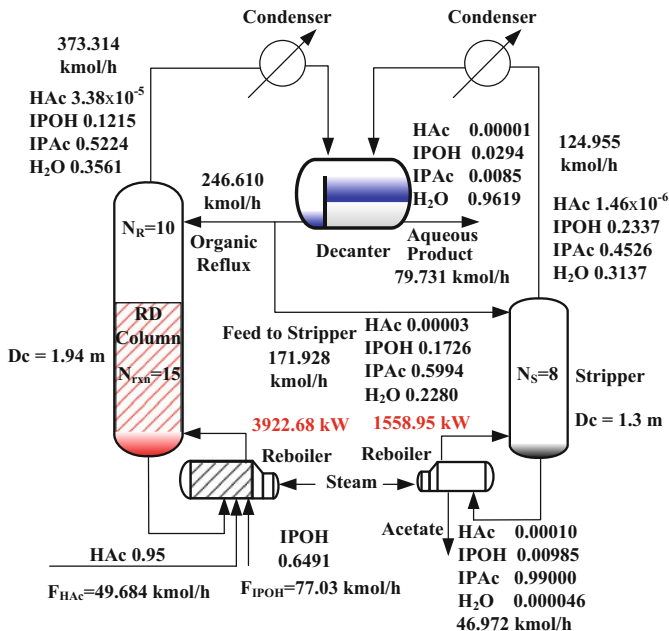


Fig. 5.28 Conventional RD configuration for IPAc process [49]

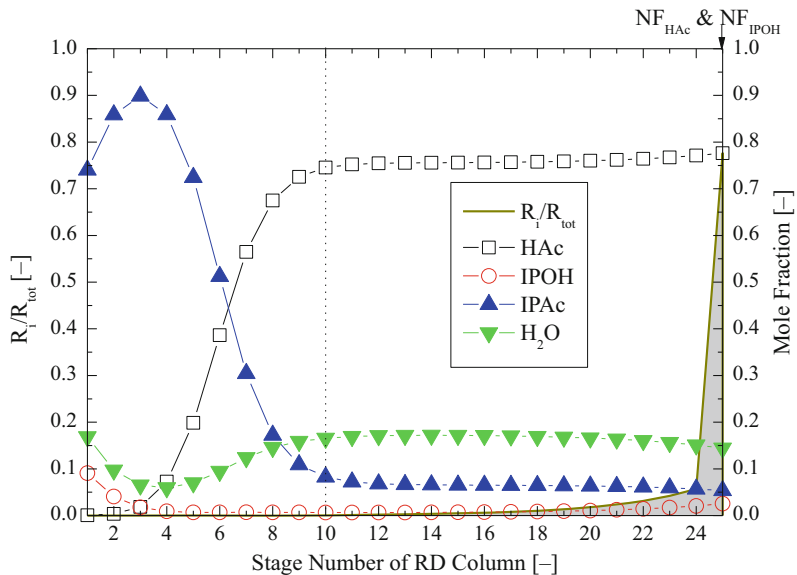
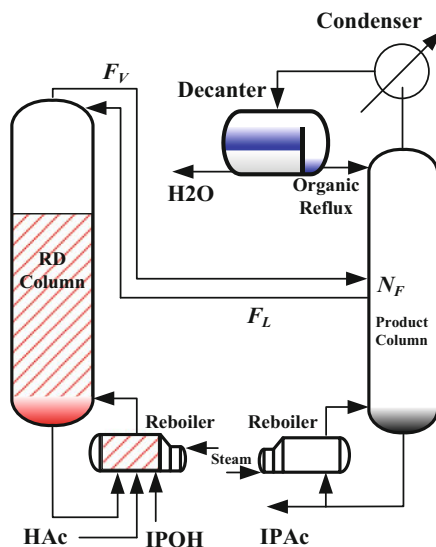


Fig. 5.29 Composition profiles of RD column for conventional IPAc RD configuration [49]

Fig. 5.30 Thermally coupled configuration for IPAc process



to carry more water towards the top of the column; thus, a liquid side draw from the product column is designed. To complete the thermally coupled configuration, the condenser in the RD column is removed and the vapor stream from the overhead is input to the same side draw location at the product column.

In Fig. 5.30, the reboiler duty of the right side product column is an operating variable used to meet the purity of IPAc, and the liquid side draw flow rate is used to maintain the HAc impurity in the product stream. The only design variable is the “vapor–liquid exchange location” (NF) in order to minimize the energy requirement.

The optimization procedure is shown as follows:

1. Initialize the NF.
2. Adjust the FL and reboiler duty of the right side column until the product specifications are met.
3. Go back to step 1 and change NF until the reboiler duty of overall process is minimized.

By following the optimization procedure, the best vapor–liquid exchange locations are at stage 5. Although the RD column reboiler duty remained about the same when the vapor–liquid exchange location varies, the separation column reboiler duty is minimum at the fifth tray when the vapor–liquid exchange location was varied.

The detailed results of the IPAc process with thermally coupled RD are shown in Fig. 5.31. The RD column reboiler duty is 3947.42 kW which is almost the same as in Fig. 5.28. However, the product column reboiler duty is only 265.67 kW, which is significantly lower than the stripper reboiler duty (1558.95 kW) of the conventional RD configuration. The optimal total reboiler duty of the thermally coupled

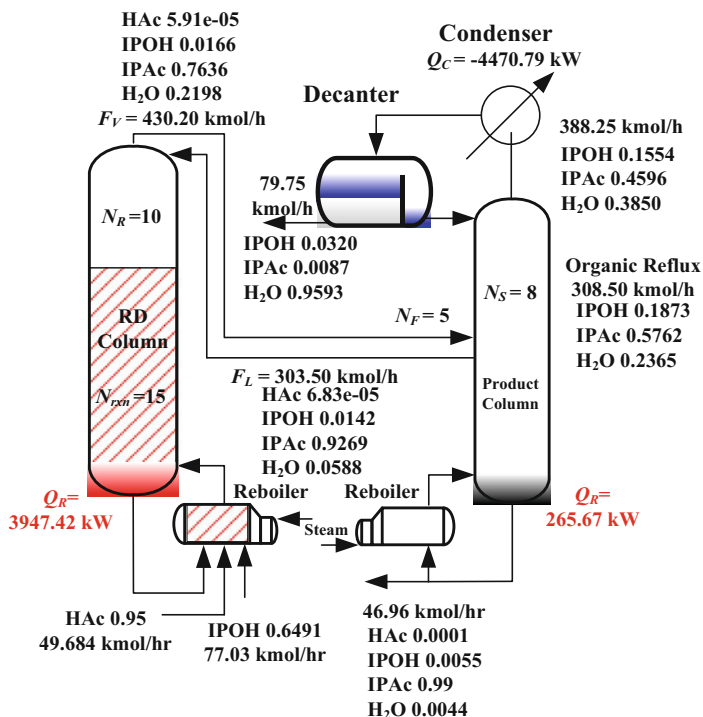


Fig. 5.31 Optimal results of the thermally coupled RD for IPAc process

RD is 23.14 % less than the conventional RD system. The liquid composition profile of the thermally coupled RD for this process is shown in Fig. 5.32. Comparing the composition of IPAc in the upper section of the RD column in the thermally coupled RD with that of the conventional RD configurations, the remixing effect is clearly eliminated because the IPAc composition increases steadily towards the top in the thermally coupled RD column. Another interesting observation in the composition profile can be made from the projection of the tetrahedron three-dimensional space to a two-dimensional space by using the composition variable transformation method [39]. The distillation path of the tray liquid and vapor compositions in the coordinate of composition variable transformation space is shown in Fig. 5.33 and has been demonstrated by Lee et al. [50].

Figure 5.33 also shows the tie lines and the compositions of the organic and aqueous phases. The curves with triangular symbols denote the composition trajectory of the RD column composition profile, and the curves with circles denote the composition trajectory of the product column. In Fig. 5.33a, the vapor and liquid composition trajectories in the conventional RD column show an evident turn in the two composition profiles. In Fig. 5.33b, the turn in the composition trajectories for the thermally coupled RD is eliminated. Additionally, the composition trajectories of the vapor and liquid for the product column with thermally coupled configuration

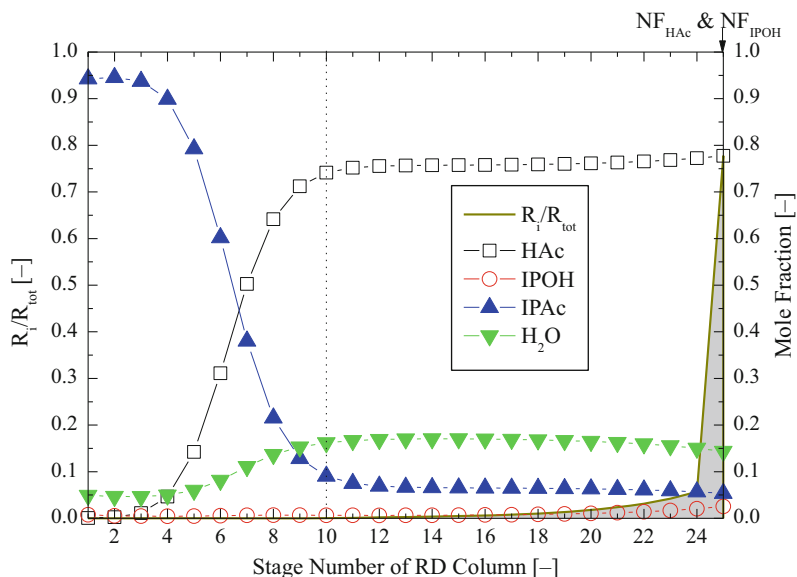


Fig. 5.32 Composition profiles of RD column for thermally coupled IPAc RD configuration

all show a more linear behavior than the stripper in the conventional RD system. This more linear behavior of the composition trajectory in this transformation coordinate hints at the energy saving in the product column.

In this section, the potential energy savings of the thermally coupled RD is introduced for IPAc system. The thermally coupled configuration includes moving the location of the decanter to the stripper side, totally refluxing the organic phase outlet stream, and adding a side draw liquid stream from the stripper to the RD column. The simulation result shows that 23.14 % energy savings can be realized by using the thermally coupled configuration.

5.5.4 Heat-Integrated Reactive Systems with Multiple Effect

For the multi-effect distillations, heat integration utilizes the heat of top distillate vapor in one column to supply the heat to the reboiler of next column. In order to provide the necessary temperature difference, the columns are operated under different pressures. In this section, the hydrolysis of Methyl Acetate and esterification of Isopropyl Acetate are chosen to illustrate the use of multi-effect distillation in reactive processes.

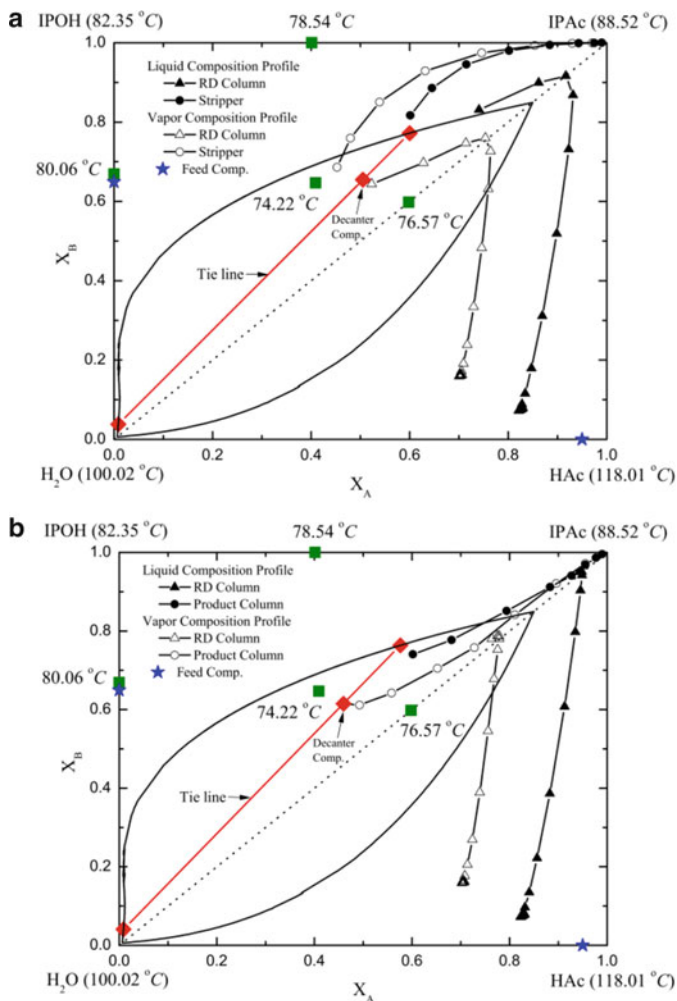


Fig. 5.33 Composition trajectories of IPAC process: transformed liquid and vapor composition in the quaternary system ($X_A = X_{HAc} + X_{IPAc}$, $X_B = X_{IPOH} + X_{IPAc}$) for (a) conventional RD configuration, (b) thermally coupled RD configuration [50]

5.5.4.1 Multiple Effect Process for the Hydrolysis of Methyl Acetate

The concept of the multi-effect distillation column entails splitting the feed stream into two smaller reactive distillation columns operated at different pressures. The operating pressure of the high-pressure column is determined so that the heat removal at the condenser of the high-pressure column can be matched to the heat input at the reboiler of the low-pressure column, thus, energy savings can be achieved by means of heat integration. It is worthy to mention that the boiling

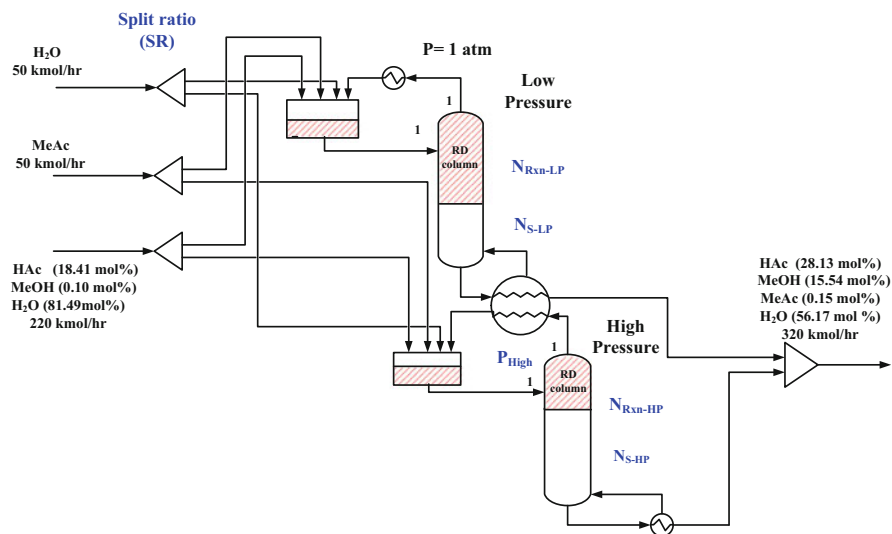


Fig. 5.34 Conceptual design of the multi-effect reactive distillation system [44]

point ranking of this RD system should not change due to the pressure increase in RD column (see Table 5.7).

Figure 5.34 shows the conceptual flowsheet of the reactive multi-effect configuration. The low-pressure column is assumed to operate at atmospheric pressure. The design variables include operating pressure at high-pressure column (P_{High}), stripping stages in the high-pressure column ($N_{S\text{-HP}}$), reactive stages in the high-pressure column ($N_{\text{Rxn-HP}}$), stripping stages in the low-pressure column ($N_{S\text{-Low P}}$), reactive stages in the low-pressure column ($N_{\text{Rxn-LP}}$), and the feed-splitting ratio (SR). The methyl acetate composition at the combined columns bottom is specified at 0.15 mol% by varying the reboiler duty of the high-pressure column.

The upper limit for the operation pressure of the reactive distillation is 8 atm to avoid a side reaction that generates dimethyl ether. The operating temperature in the reaction section has to be lower than 120 °C to meet the catalyst (Amberlyst® 15) operation conditions. The minimum temperature difference for feasible heat exchange between the condenser of the high-pressure and the reboiler of the low-pressure column is 10 °C.

For determining the optimal values of the six design variables, an iterative sequential optimization search procedure was adopted. The objective function is to minimize the TAC. The steam prices of high-pressure column and low-pressure column are 3.04 (\$/1000 lb) and 2.28 (\$/1000 lb), respectively. The catalyst cost is assumed to be \$3.5/lb and to be replaced every 3 months. The payback of 3 years ($\theta = 3$) is assumed. The equipment cost was calculated according to Douglas's textbook [52].

The optimal values for the six design variables are: high-pressure column operated at 4.6 atm, 17 total stages of the high-pressure column, 2 reactive stages

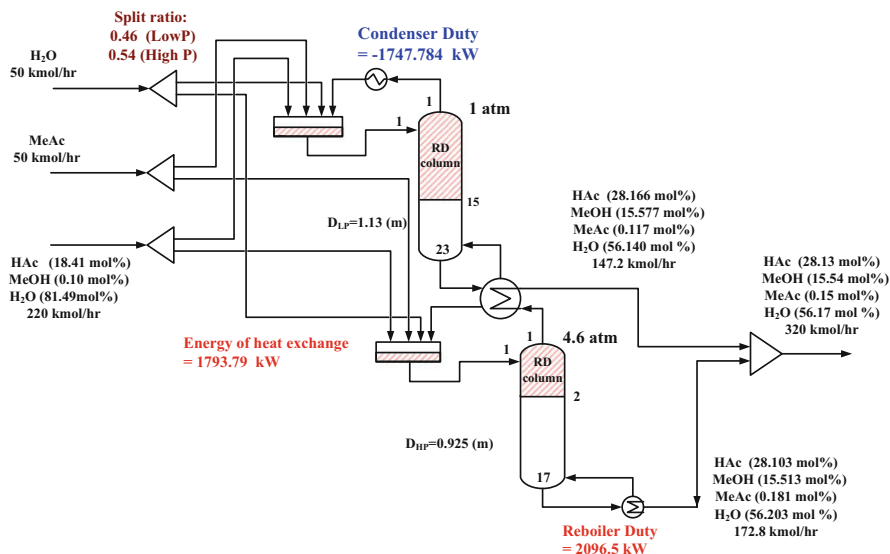


Fig. 5.35 Optimal flowsheet of the reactive multi-effect design for RD column

of the high-pressure column, 23 total stages of the low-pressure column, 15 reactive stages of the low-pressure column, and the feed-splitting ratio at 0.54.

Figure 5.35 shows the resulting optimal flowsheet for this feed-splitting heat integration configuration (reactive multi-effect). The detailed comparison of this reactive multi-effect configuration to the original configuration without heat integration shows that the energy saving and the operating cost saving of this heat integration configuration are at 38.26 % and 15.19 %, respectively. The cost of this reactive multi-effect configuration only increases slightly and the TAC is still lower than the original configuration without heat integration by 6.42 %.

Figure 5.36 shows the composition and reaction profiles of the two RD columns shown in Fig. 5.35. For each column, most of the reaction takes place at the reflux drum. The MeAc composition diminishes at each column bottom as it was specified. Notice that under the optimal condition, the shaded area in Fig. 5.36 displays that over 90 % of the reaction takes place in the high-pressure reflux drum; however, only about 70 % of the reaction takes place in the low-pressure reflux drum.

5.5.4.2 Multiple Effect Process for the Esterification of Isopropyl Alcohol

The base case of isopropyl alcohol reactive distillation configuration was taken from Lai et al. [49]. Thermodynamic and kinetic models are shown in previous sections. The original design of Isopropyl acetate reactive distillation configuration

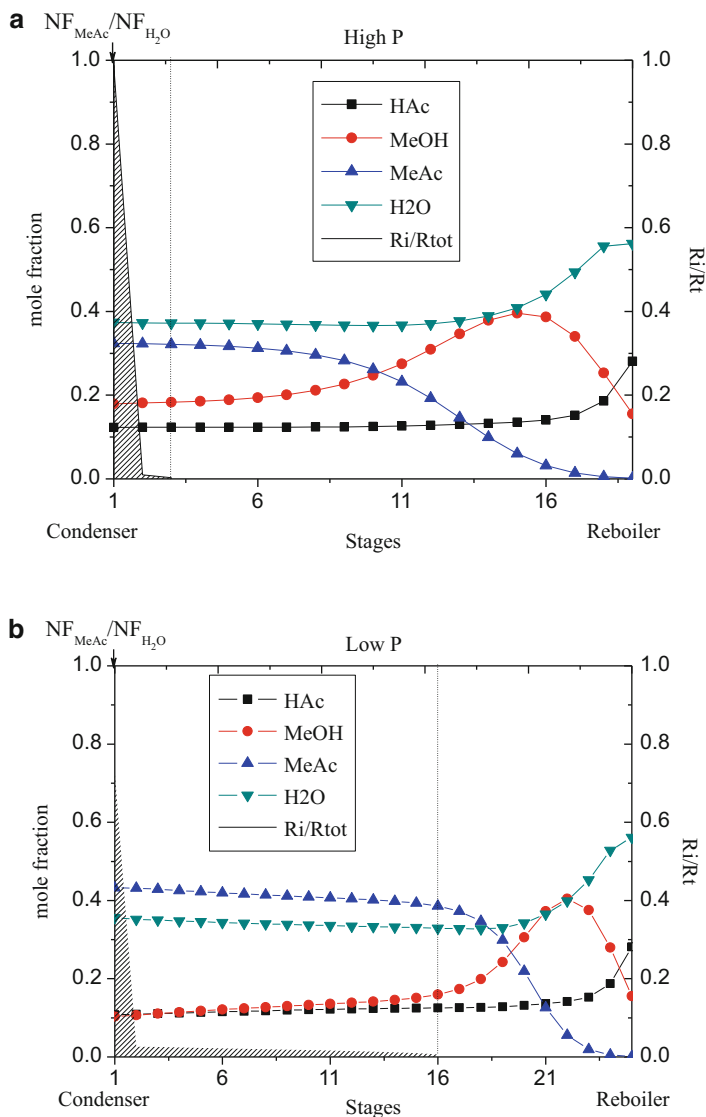


Fig. 5.36 Composition profile. (a) High-pressure RD. (b) Low-pressure RD [44]

contains a reactive column with a decanter and a stripping column. The lower part of the reactive column is the reaction section and the upper part of the reactive column is the rectifying section, with both pressures at 1.2 atm. Acetate and isopropanol are fed to the bottom. Acetic acid has the highest boiling point in this case. In order to avoid materials loss, there is no product coming out from the bottom. In the original reactive distillation configuration, the removed energy from

the condenser at the top is greater than the energy supplied to the reboiler at the bottom. However, the temperature in the top is lower than the temperature in the bottom. Therefore, heat transfer is infeasible.

In order to transfer heat from condenser to reboiler in the reactive distillation column, it is necessary to increase the pressure in the reactive distillation column. The pressure increase will affect the performance in the reaction and separation sections. High-pressure distillation column will result in higher operating temperatures, which speed up the reaction rate and the reaction system moves towards the equilibrium faster. Therefore, the overall effect resulted from increasing the pressure is beneficial.

When the top pressure of the reaction column is higher than 2.7 atm, the temperature difference between top and bottom in the reactive distillation column is higher than the minimum heat transfer temperature difference ($\Delta T_{\min} = 10\text{ }^{\circ}\text{C}$), which implies that heat can effectively be transferred. Figure 5.37 shows the design results for the multi-effect configuration. The energy consumption of multi-effect was reduced from 5481.63 kW to 3766.5 kW, which results in 31.3 % energy savings.

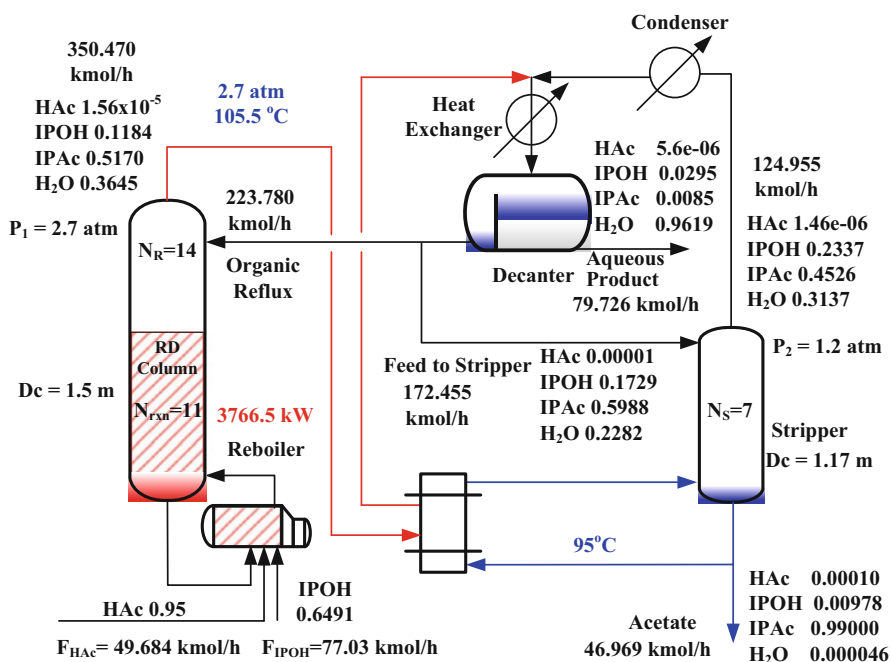


Fig. 5.37 Isopropyl acetate RD process for multi-effect configuration

5.5.5 Energy Saving and Cost Comparisons of Whole Two Configurations

5.5.5.1 Process Comparison for the Hydrolysis of Methyl Acetate

Table 5.12 is a comprehensive table that summarizes the energy consumption and TAC for the original RD configuration, multi-effect configuration and thermally coupled configuration. Compared with the original RD configuration, the reactive multi-effect configuration can save energy and this type of heat integration is very common in the industry. However, the main drawback is that the multi-effect reactive distillation needs to use high-pressure steam to supply energy at the reboiler. As a result, it only saves 2.84 % of the TAC for the overall process including two separation columns. The thermally coupled configuration saves 31.57 % energy compared with the original RD configuration. The reason is because the thermally coupled configuration can eliminate the remix effect in the columns bottom. The heat integration of thermally coupled configuration can also save energy. Overall, the TAC of thermally coupled configuration can still save 11.10 % energy consumption compared with the original RD configuration.

5.5.5.2 Process Comparison for the Esterification of Isopropyl Alcohol

Table 5.13 is a comparison table that summarizes the energy consumption of isopropyl alcohol for the original reactive distillation configuration, multi-effect configuration and thermally coupled configuration. For the original reactive distillation configuration, the thermally coupled of reactive distillation configuration can save 23.14 % of the energy consumption in the overall energy use. The reason is the

Table 5.12 Hydrolysis of methyl acetate's energy consumption and TAC comparison of RD versus multi-effect and thermally coupled

Framework	Energy consumption (kW)	TAC (\$1000/year)	Energy saving (%)	TAC saving (%)
RD	8403.07	1824.48	–	–
Multi-effect	7104.11	1772.63	15.46	2.84
Thermally coupled	5750	1622.04	31.57	11.10

Table 5.13 Esterification of isopropyl alcohol's energy consumption comparison of RD versus multi-effect and thermally coupled

Framework	Energy consumption (kW)	Energy saving (%)
RD	5481.63	–
Thermally coupled	4213.09	23.14
Multi-effect	3766.5	31.28

thermally coupled configuration can eliminate the remixing effect in the bottom. The multi-effect via reactive distillation configuration can save 31.28 % more energy than the original reactive distillation configuration. However, operation at higher pressure is required. Caution must be taken to apply this arrangement because it may result in catalyst deactivation or decomposition due to higher temperature and pressure conditions.

5.6 Future Directions in Heat-Integrated Intensified Distillation Processes

The advantages of heat-integrated distillation at stages over typical condenser-reboiler heat integration in terms of energy consumption and TAC have been shown in this chapter. As the complexity of intensified distillation increases, the development of efficient and reliable optimization approaches is necessary. The combination of simulations, which handle nonlinear and non-convex equations such as thermodynamics and mass balances, and optimization, which is a strong tool to find optimal locations and heat load in heat-integrated distillation, can be superior to approaches based on only simulations or optimization. In addition, MIP, MINLP, or stochastic optimization methods can be interchanged according to the users' skills and preferences.

Figure 5.38 shows a qualitative comparison of several approaches to find heat-integrated intensified distillation. Although simulation driven approaches can handle a large number of components, the simulation time and the lack of robustness to find a global optimum solution are the two main drawbacks. For optimization driven approaches, so far they have been used for the separation of binary mixtures or separations done in one column. Simulation/optimization approaches for the separation of multicomponent mixtures is one topic that needs further research.

The presented cases were optimized at steady state; however, dynamic optimization and the controllability assessment of heat-integrated intensified distillation is also an open field that needs further study.

It is easy to envision that the process dynamic response of heat-integrated configurations will be more oscillatory than conventional distillation due to the compactness in process flowsheet and/or less control degree of freedom.

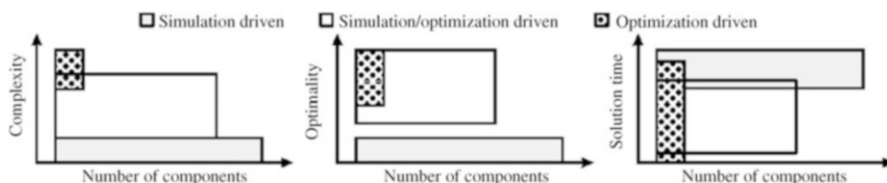


Fig. 5.38 Simulation and optimization approaches for heat-integrated intensified distillation

Regarding thermally coupled configuration, the control of the sidedraw flows is an important issue especially when the sidedraw is withdrawn as vapor. Luyben [55] proposed a concept of “pressure-compensated temperature” to adjust the temperature control loop as a function of the top pressure of a column. Straightforward PID control might not be enough to control the process; therefore, pressure-compensated control, cascade control, and nonlinear control techniques might be necessary.

Regarding thermally coupled configuration, the control of the sidedraw flows is an important issue especially when the sidedraw is withdrawn as vapor. Unlike liquid sidedraws, vapor sidedraws are not easy to control due to the pressure fluctuation of the column.

The effect of heat-integrated intensified distillation in arising multiple steady-states has not been evaluated. This also shows an open area to further research the presented ideas. The implementation of lab scale or bench scale to validate the theoretical foundations of heat-integrated distillation is another area that needs to be explored.

5.7 Concluding Remarks

The presented ideas related to the further intensification of complex distillation by means of heat integration can be useful for engineers and researchers in the field of process systems engineering.

Heat integration is preferred for clean services, for geographical regions where fuel and electricity prices are expensive, or for processes at atmospheric or subatmospheric pressure to prevent the deposition of solid particles.

Although the energy consumption can be reduced, the implementation of heat-integrated intensified distillation processes can be limited because two main reasons:

1. The use of expensive utilities (i.e., high-pressure steam) can reduce the economic savings. This was demonstrated in this chapter. The intensification of reactive distillation results in higher operating costs.
2. The use of complex control configurations due to high process interaction between the vapor and liquid streams involved in heat integration.

The first reason is related with the steady-state design and optimization while the second reason is related with the dynamic state operation and selection of controlled and manipulated variables. One way to deal with the aforementioned limitations is to simultaneously optimize the design and control in intensified distillation. Therefore, new approaches handling this issue are urged in order to bust the implementation of intensified processes.

The presented ideas can be extended to multicomponent mixtures and reactive systems involving more reactions without lack of generality.

References

1. Alcántara-Avila JR, Hasebe S, Kano M (2013) New synthesis procedure to find the optimal distillation sequence with internal and external heat integrations. *Ind Eng Chem Res* 52 (13):4851–4862. doi:[10.1021/ie302863p](https://doi.org/10.1021/ie302863p)
2. Alcántara-Avila JR (2012) Process intensification in distillation sequences. Dissertation, Kyoto University
3. Harwardt A, Marquardt W (2012) Heat-integrated distillation columns: vapor recompression or internal heat integration? *AIChE J* 58(12):3740–3750. doi:[10.1002/aic.13775](https://doi.org/10.1002/aic.13775)
4. Wang Y, Huang K, Wang S (2010) A simplified scheme of externally heat-integrated double distillation columns (EHIDDiC) with three external heat exchangers. *Ind Eng Chem Res* 49 (7):3349–3364. doi:[10.1021/ie901534q](https://doi.org/10.1021/ie901534q)
5. Kiss AA, Flores Landaeta SJ, Infante Ferreira CA (2012) Towards energy efficient distillation technologies—making the right choice. *Energy* 47:531–542. doi:[10.1016/j.energy.2012.09.038](https://doi.org/10.1016/j.energy.2012.09.038)
6. Fonyo Z, Benkő N (1998) Comparison of various heat pump assisted distillation configurations. *Chem Eng Res Des* 76(3):348–360. doi:[10.1205/026387698524776](https://doi.org/10.1205/026387698524776)
7. McCabe DL, Vivona MA (1999) Treating process wastewater employing vacuum distillation using mechanical vapor recompression. *Environ Prog* 18(1):30–33
8. Schmal JP, Van der Kooij HJ, De Rijke A et al (2006) Internal versus external heat integration operational and economic analysis. *Chem Eng Res Des* 84(A5):374–380. doi:[10.1205/cherd05041](https://doi.org/10.1205/cherd05041)
9. Alcántara-Avila JR, Gómez-Castro FI, Segovia-Hernández JG et al (2014) Optimal design of cryogenic distillation columns with side heat pumps for the propylene/propane separation. *Chem Eng Process* 82:112–122. doi:[10.1016/j.cep.2014.06.006](https://doi.org/10.1016/j.cep.2014.06.006)
10. Seider WD, Seader JD, Lewin DR, Widagdo S (2010) Product and process design principles: synthesis, analysis, and evaluation. Wiley, Asia
11. IEA (2012) Energy balances of non-OECD countries 2012. OECD, Paris, http://dx.doi.org/10.1787/energy_bal_non-oecd-2012-en
12. Ministry of Economy, Trade and Industry (2014) Nihon no enerugi 2014 (The energy in Japan 2014). http://www.enecho.meti.go.jp/about/pamphlet/pdf/energy_in_japan2014.pdf. Accessed 24 Feb 2015
13. Shenvi AA, Herron DM, Agrawal R (2011) Energy efficiency limitations of the conventional heat integrated distillation column (HIDiC) configuration for binary distillation. *Ind Eng Chem Res* 50(1):119–130. doi:[10.1021/ie101698f](https://doi.org/10.1021/ie101698f)
14. Mah RSH, Nicholas JJ, Wodnik RB (1977) Distillation with secondary Reflux and vaporization: a comparative evaluation. *AIChE J* 23:651–657
15. Nakaiwa M, Huang K, Endo A et al (2003) Internally heat-integrated distillation columns: a review. *Chem Eng Res Des* 81(1):162–177. doi:[10.1205/026387603321158320](https://doi.org/10.1205/026387603321158320)
16. Ho TJ, Huang CT, Lee LS et al (2010) Extended Ponchon-Savarit method for graphically analyzing and designing internally heat-integrated distillation columns. *Ind Eng Chem Res* 49 (1):350–358. doi:[10.1021/ie9005468](https://doi.org/10.1021/ie9005468)
17. Shahandeh H, Ivakpour J, Kasiri N (2014) Internal and external HIDiCs (heat-integrated distillation columns) optimization by genetic algorithm. *Energy* 64(1):875–886. doi:[10.1016/j.energy.2013.10.042](https://doi.org/10.1016/j.energy.2013.10.042)
18. Suphanit B (2010) Design of internally heat-integrated distillation column (HIDiC): uniform heat transfer area versus uniform heat distribution. *Energy* 35(3):1505–1514. doi:[10.1016/j.energy.2009.12.008](https://doi.org/10.1016/j.energy.2009.12.008)
19. Olujic Z, Fakhri F, de Rijke A et al (2003) Internal heat integration—the key to an energy-conserving distillation column. *J Chem Technol Biotechnol* 78(2–3):241–248. doi:[10.1002/jctb.761](https://doi.org/10.1002/jctb.761)
20. Olujic Z, Sun L, de Rijke A et al (2006) Conceptual design of an internally heat integrated propylene-propane splitter. *Energy* 31(15):3083–3096. doi:[10.1016/j.energy.2006.03.030](https://doi.org/10.1016/j.energy.2006.03.030)

21. Olujic Z, Sun L, Gadalla A et al (2008) Enhancing thermodynamic efficiency of energy intensive distillation columns via internal heat integration. *Chem Biochem Eng Q* 22 (4):383–392
22. Horiuchi K, Yanagimoto K, Kataoka K (2008) Energy saving characteristics of the internally heat integrated distillation column (HIDiC) pilot plant for multicomponent petroleum distillation. *J Chem Eng Jpn* 41(8):771–778
23. Cabrera-Ruiz J, Jiménez-Gutiérrez A, Segovia-Hernández JG (2011) Assessment of the implementation of heat-integrated distillation columns for the separation of ternary mixtures. *Ind Eng Chem Res* 50(4):2176–2181. doi:[10.1021/ie101939e](https://doi.org/10.1021/ie101939e)
24. Kataoka K, Noda H (2014) Naibu netsukokan Shiki joryuto (HIDiC) no gijutsu Kaihatsu (technological development of internal heat-integrated distillation column (HIDiC)). *Synthesiology* 7(3):163–178
25. Ho TJ, Huang CT, Lin JM et al (2009) Dynamic simulation for internally heat-integrated distillation columns (HIDiC) for propylene–propane system. *Comput Chem Eng* 33:1187–1201. doi:[10.1016/j.compchemeng.2009.01.004](https://doi.org/10.1016/j.compchemeng.2009.01.004)
26. Huang K, Shan L, Zhu Q et al (2007) Design and control of an ideal heat-integrated distillation column (ideal HIDiC) system separating a close-boiling ternary mixture. *Energy* 32 (11):2148–2156. doi:[10.1016/j.energy.2007.04.007](https://doi.org/10.1016/j.energy.2007.04.007)
27. Kano M, Fukushima T, Makita H et al (2007) Multiple steady-states in a heat integrated distillation column (HIDiC). *J Chem Eng Jpn* 40(10):824–831. doi:[10.1252/jcej.06WE278](https://doi.org/10.1252/jcej.06WE278)
28. Wakabayashi T, Hasebe S (2011) Naibu netsukokan gata joryuto (HIDiC) ni okeru naibu netsukokan ryobunpu no shoenerugi Seino ni ataeru ekyo (effect of internal heat exchange rate distribution on energy saving in heat integrated distillation column (HIDiC)). *Kagaku Kogaku Ronbunshu* 37(6):499–505
29. Wakabayashi T, Hasebe S (2013) Design of heat integrated distillation column by using H-xy and T-xy diagrams. *Comput Chem Eng* 56:174–183. doi:[10.1016/j.compchemeng.2013.05.020](https://doi.org/10.1016/j.compchemeng.2013.05.020)
30. Mane A, Jana AK (2010) A new intensified heat integration in distillation column. *Ind Eng Chem Res* 49(19):9534–9541. doi:[10.1021/ie100942p](https://doi.org/10.1021/ie100942p)
31. Kiran B, Jana AK, Samanta AN (2012) A novel intensified heat integration in multicomponent distillation. *Energy* 41(1):443–453. doi:[10.1016/j.energy.2012.02.055](https://doi.org/10.1016/j.energy.2012.02.055)
32. Taseibunkei naibu-netsukokanshiki joryu-sochi (Internal heat integrated distillation system for multi-component distillation). Patent No. 4819756
33. Kataoka K, Noda H, Yamaji H et al (2009) A compressor-free HIDiC system for recovery of waste solvent mixtures. Paper presented at 8th World Congress of chemical engineering, Montreal, Canada, 23–27 August 2009
34. Kataoka K, Noda H, Yamaji H et al (2009) Heat transfer and flow characteristics of a double-tube HIDiC trayed column. Paper presented at 8th World Congress of chemical engineering, Montreal, Canada, 23–27 August 2009
35. Zhang X, Huang K, Chen H et al (2011) Comparing three configurations of the externally heat-integrated double distillation columns (EHIDDiCs). *Comput Chem Eng* 35(10):2017–2033. doi:[10.1016/j.compchemeng.2010.11.008](https://doi.org/10.1016/j.compchemeng.2010.11.008)
36. Miyazaki A, Alcántara-Avila JR, Sotowa KI, Horikawa T (2014) Trade-off assessment between controllability and energy savings in internally and externally heat integrated distillation structures. Paper presented at the 5th international symposium on advanced control of industrial processes, Hiroshima, Japan, 28–30 May 2014
37. Alcántara-Avila JR, Sotowa KI, Horikawa T (2014) Iterative procedure for updating the temperature profile in distillation columns with heat-integrated stages. Paper presented at 10th international conference on separation science and technology (ICSST14), Nara, Japan, 30 October–1 November 2014
38. Alcántara-Avila JR, Hasebe S (2013) Hierarchical synthesis procedure of optimal distillation sequences with internal and external heat integrations. Paper presented at 9th World Congress of chemical engineering, Seoul, South Korea, 18–23 August 2014

39. Malone MF, Doherty MF (2000) Reactive distillation. *Ind Eng Chem Res* 39:3953–3957
40. Luyben WL, Yu CC (2008) Reactive distillation design and control. Wiley, Hoboken
41. Sundmacher K, Kienle A (eds) (2003) Reactive distillation: status and future directions. Wiley-VCH Verlag GmbH & Co. KGaA, Weinheim, Germany
42. Lin YD, Chen JH, Cheng JK et al (2008) Process alternatives for methyl acetate conversion using reactive distillation. 1. Hydrolysis. *Chem Eng Sci* 63(6):1668–1682. doi:[10.1016/j.ces.2007.11.009](https://doi.org/10.1016/j.ces.2007.11.009)
43. Lin YD (2012) Design and control of a reactive distillation process for methyl acetate hydrolysis. Dissertation, Master thesis, National Taiwan University
44. Lee HY, Lee YC, Chien IL, Huang HP (2010) Design and control of a heat integrated reactive distillation system for the hydrolysis of methyl acetate. *Ind Eng Chem Res* 49:7398–7411. doi:[10.1021/ie9016754](https://doi.org/10.1021/ie9016754)
45. Pöpkén T, Götzé L, Gmehling J (2000) Reaction kinetics and chemical equilibrium of homogeneously and heterogeneously catalyzed acetic acid esterification with methanol and methyl acetate hydrolysis. *Ind Eng Chem Res* 39(7):2601–2611. doi:[10.1021/ie000063q](https://doi.org/10.1021/ie000063q)
46. Pöpkén T, Steinigeweg S, Gmehling J (2001) Synthesis and hydrolysis of methyl acetate by reactive distillation using structured catalytic packings: experiments and simulation. *Ind Eng Chem Res* 40(6):1566–1574. doi:[10.1021/ie0007419](https://doi.org/10.1021/ie0007419)
47. Hayden JG, O'Connell JP (1975) A generalized method for predicting second virial coefficients. *Ind Eng Chem Process Des Dev* 14(3):209–216. doi:[10.1021/i260055a003](https://doi.org/10.1021/i260055a003)
48. Tang YT, Chen YW, Huang HP et al (2005) Design of reactive distillations for acetic acid esterification with different alcohols. *AIChE J* 51(6):1683–1699. doi:[10.1002/aic.10519](https://doi.org/10.1002/aic.10519)
49. Lai IK, Liu YC, Yu CC et al (2008) Production of high-purity ethyl acetate using reactive distillation: experimental and start-up procedure. *Chem Eng Process* 47(9–10):1831–1843. doi:[10.1016/j.cep.2007.10.008](https://doi.org/10.1016/j.cep.2007.10.008)
50. Lee HY, Lai IK, Huang HP, Chien IL (2012) Design and control of thermally coupled reactive distillation for the production of isopropyl acetate. *Ind Eng Chem Res* 51:11753–11763. doi:[10.1021/ie300647h](https://doi.org/10.1021/ie300647h)
51. Gadewar SB, Malone MF, Doherty MF (2002) Feasible region for a countercurrent cascade of vapor-liquid CSTRs. *AIChE J* 48(4):800–814. doi:[10.1002/aic.690480414](https://doi.org/10.1002/aic.690480414)
52. Sander S, Flisch C, Geissler E, Schoenmakers H et al (2007) Methyl acetate hydrolysis in a reactive divided wall column. *Chem Eng Res Des* 85(1):149–154. doi:[10.1205/cherd06106](https://doi.org/10.1205/cherd06106)
53. Douglas JM (1998) Conceptual design of chemical processes. McGraw-Hill, New York
54. Tedder DW, Rudd DF (1978) Parametric studies in industrial distillation: part 1 design comparisons. *AIChE J* 24:303–315. doi:[10.1002/aic.690240220](https://doi.org/10.1002/aic.690240220)
55. Luyben WL (2008) Design and control of a fully heat-integrated pressure-swing azeotropic distillation system. *Ind Eng Chem Res* 47(8):2681–2695. doi:[10.1021/ie071366o](https://doi.org/10.1021/ie071366o)
56. Horsley LH (1973) Azeotropic data—III, Advances in chemistry series no.116. American Chemical Society, Washington, DC